Seong Beom Lee
Department of Chemical Engineering,
University of Washington,
Seattle, WA 98195
e-mail: Seongl2@uw.edu

Kishalay Mitra
Department of Chemical Engineering,
Indian Institute of Technology Hyderabad,
Kandi, Sangareddy 502285, Telangana, India
e-mail: kishalay@iith.ac.in

Harry D. Pratt III
Sandia National Laboratories,
Albuquerque, NM 87185
e-mail: hdpratt@sandia.gov

Travis M. Anderson
Sandia National Laboratories,
Albuquerque, NM 87185
e-mail: tmander@sandia.gov

Venkatasailanathan Ramadesigan
Department of Energy Science and Engineering,
Indian Institute of Technology Bombay,
Powai 400076, Mumbai, Maharashtra, India
e-mail: venkatr@iitb.ac.in

Babu R. Chalamala
Sandia National Laboratories,
Albuquerque, NM 87185
e-mail: bchalam@sandia.gov

Venkat R. Subramanian[1]
Department of Chemical Engineering,
University of Washington,
Seattle, WA 98195;
Pacific Northwest National Laboratory,
Richland, WA 99354
e-mail: vsubram@uw.edu

Open Data, Models, and Codes for Vanadium Redox Batch Cell Systems: A Systems Approach Using Zero-Dimensional Models

In this paper, we study, analyze, and validate some important zero-dimensional physics-based models for vanadium redox batch cell (VRBC) systems and formulate an adequate physics-based model that can predict the battery performance accurately. In the model formulation process, a systems approach to multiple parameters estimation has been conducted using VRBC systems at low C-rates (~C/30). In this batch cell system, the effect of ions' crossover through the membrane is dominant, and therefore, the capacity loss phenomena can be explicitly observed. Paradoxically, this means that using the batch system might be a better approach for identifying a more suitable model describing the effect of ions transport. Next, we propose an efficient systems approach, which enables to help understand the battery performance quickly by estimating all parameters of the battery system. Finally, open source codes, executable files, and experimental data are provided to enable people's access to robust and accurate models and optimizers. In battery simulations, different models and optimizers describing the same systems produce different values of the estimated parameters. Providing an open access platform can accelerate the process to arrive at robust models and optimizers by continuous modification from the users' side.
[DOI: 10.1115/1.4044156]

Introduction

Redox flow batteries (RFBs) are promising energy storage systems for grid/microgrid applications [1]. There has been significant technological progress in the recent past toward meeting the growing need for large-scale energy storage systems such as RFBs [2]. Among different types of RFBs, vanadium redox flow batteries (VRFBs) have gained more attention, and as a result, several physics-based electrochemical models for these systems describing the battery operations have been developed.

Physics-based VRFB models can be classified by dimensions, from zero- to two-dimensional models, which are listed in Table 1. Models in each category have their own advantages and can be used depending on the users' needs. For example, zero-dimensional models have been developed to be easily

implementable, enabling to quickly understand, predict, and control the battery system [3,6,7]. Multidimensional models have been implemented by including more detailed physics of the system [12]. As described in Table 1, the current trend is to include detailed physical phenomena, such as transport of ions and side reactions of the system [10,11], and therefore, models with more complexities have been built. A zero-dimensional model was developed for batch cell systems including diffusion of vanadium ions through the membrane [4], and this was the first attempt to simulate vanadium ions' crossover through the membrane [4]. The model was further enhanced to include all ions and transport properties of the system [6,12,13]. One-dimensional membrane models, which are based on dilute and concentrated solution theories, have been developed [8,9]. In the one-dimensional membrane models, the membrane region is simplified to one dimension assuming bulk electrolytes at the positive and negative electrodes. Also, VRFB models have been developed in two dimensions to include diffusion, migration, and convection of all ions and detailed physics of the system [12].

In this paper, we study and analyze vanadium redox batch cell (VRBC) systems at low C-rates with zero-dimensional physics-based models using a systems approach, providing experimental data, models, and codes. There are three objectives:

**Table 1 Selected physics-based electrochemical engineering models of vanadium redox flow batteries**

Model	V^{2+}	V^{3+}	VO^{2+}	VO_2^+	H^+	OH^-	HSO_4^-	SO_4^{2-}	H_2O	Across: Diff.	Mig.	Conv.	Membrane: Diff.	Mig.	Conv.	H_2	O_2	Thermal effects	Transport theory	Key points	Reference (year)
Zero-dimensional models																					
Shah et al.	O	O	O	O	O	X	X	X	O	N/A: Zero-dimensional models assume that bulk electrolyte transport happens across the membrane from positive to negative electrolytes or from negative to positive electrolytes. There are more detailed physics in real systems, but zero-dimensional models are important for control and prediction for long cycles			X H^+: No constraints for transport H_2O: Osmotic drag	X	X	X	X	Isothermal	N/A	Allowed only H^+ and H_2O crossover through the membrane	[3] (2011)
Tang et al.	O	O	O	O	X	X	X	X	X				O (Includes only V^{2+}, V^{3+}, VO^{2+}, and VO_2^+)	X	X	O	O Used current efficiency (not equations)	Isothermal	Dilute solution	Demonstrated the batch cell model	[4] (2011)
Tang et al.	O	O	O	O	X	X	X	X	X				O (Includes only V^{2+}, V^{3+}, VO^{2+}, and VO_2^+)	X	X	X	X	Thermal	Dilute solution	Coupled thermal effects with mass balance equations	[5] (2012)
Boettcher et al.	O	O	O	O	O	X	O	O	O				O (All ions except for OH^- and SO_4^{2-})	O	O	X	X	Isothermal	Dilute solution	Limitation is unidirectional flux for Mig. and Conv.	[6] (2016)
Pugach et al.	O	O	O	O	X	X	X	X	X				O (Includes only V^{2+}, V^{3+}, VO^{2+}, and VO_2^+)	O	O	X	X	Isothermal	Dilute solution	Analytical solution for ions crossover including full-directional flux	[7] (2018)
One-dimensional models (assuming bulk electrolytes at positive and negative)																					
Gandomi et al.	X	X	X	X	O	X	O	X	O	N/A: One-dimensional membrane models assume positive and negative electrolytes have bulk electrolyte transport			O (Includes only H^+, HSO_4^-, and H_2O)	O	O	X	X	Isothermal	Concentrated solution	Assumed that only H^+, HSO_4^-, and H_2O can cross the membrane	[8] (2014)
Lei et al.	O	O	O	O	O	X	O	X	X				O (All ions except for SO_4^{2-}, OH^-, and H_2O)	O	O	X	X	Isothermal	Dilute solution	Included Donnan effects	[9] (2015)
Two-dimensional models																					
Shah et al.	O	O	O	O	O	X	O	O	O	O (Includes only V^{2+}, V^{3+}, VO^{2+}, and VO_2^+)	O	O	O (Includes only H^+, HSO_4^-, and H_2O)	O	O	O	X	Isothermal	Dilute solution	No vanadium ions crossover through the membrane and side reactions of the same	[10] (2010)
Al-Fetlawi et al.	O	O	O	O	O	X	O	O	O	O (Includes only V^{2+}, V^{3+}, VO^{2+}, and VO_2^+)	O	O	O (Includes only H^+, HSO_4^-, and H_2O)	O	O	X	O	Thermal	Dilute solution		[11] (2009)
Knehr et al.	O	O	O	O	O	X	O	O	O	O (All ions except for SO_4^{2-}, and OH^-)	O	O	O	O	O	X	X	Isothermal	Dilute solution	Improved OCV and Donnan potential	[12] (2012)

Note: The symbol "O" means that ions are included in the model and the symbol "X" means ions are not included in the model. Diff., diffusion; Mig., migration; Conv., convection; OCV, open circuit voltage; N/A, not applicable.
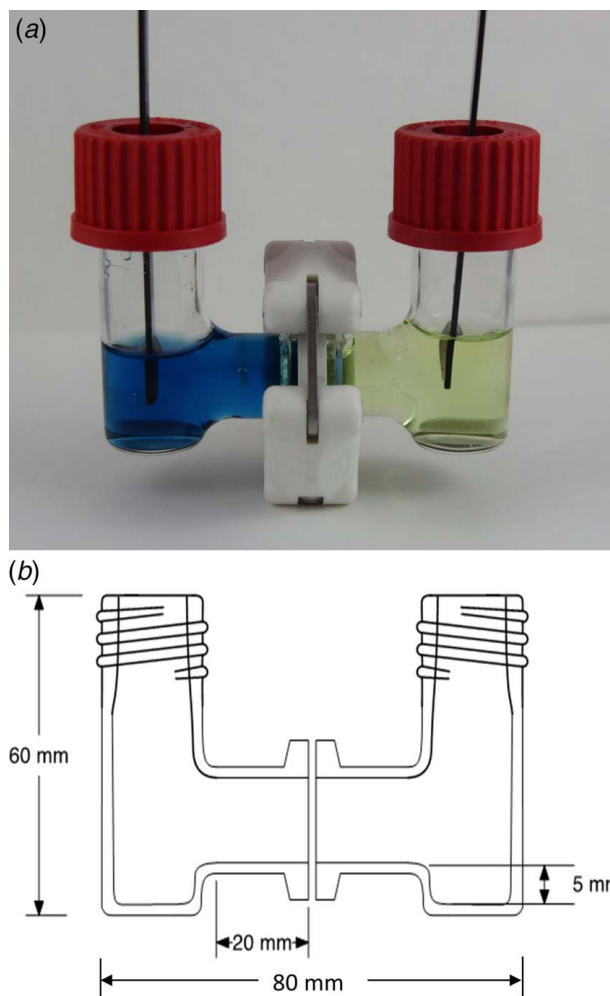
Fig. 1 Schematic of the laboratory-scale VRBC system: (a) an actual image of the system for a discharge state. The blue electrolyte represents VO^{2+} (the left chamber, positive) and the green electrolyte represents V^{3+} (the right chamber, negative) and (b) specification of the system. The batch cell system has advantages of being easy and simple to implement and a quick understanding of the performance of the RFBs. Coupling with electrochemical engineering models for the VRBC system helps modelers estimate parameters and analyze cell performance efficiently.

(i) The first objective is to validate current zero-dimensional models and to formulate a proper zero-dimensional model that can accurately predict the capacity loss phenomena of the battery system to maximize the battery usability.

The laboratory-scale batch cell system (see Fig. 1), consisting of a transparent H-cell, a membrane, electrolytes, and electrodes, has been used due to its several advantages over flow cell systems as follows: (a) coupling the batch cell with zero-dimensional models enables easy and straightforward implementation and mitigates computational challenges to simulate models and estimate their parameters [14]. (b) In this batch system, the effect of ions' crossover through the membrane is dominant at low C-rates. The ions' crossover is one of the main causes of the capacity loss of the redox flow battery systems [12]. Therefore, the capacity loss can be explicitly observed, even for a single cycle in the batch cell system at low C-rates. The study and analysis of the batch cell system based on these low C-rates will be a good starting point to build accurate zero-dimensional models for flow battery systems.

(ii) The second objective is to show that a systems approach that simultaneously estimates multiple parameters of the model allows users to quickly understand the battery system. For example, estimation of all the parameters of the physics-based model for the VRBC system has been addressed using two-cell systems, which include two different membranes, assuming that both systems have some common characteristics, such as kinetics at the electrodes, the formal potential, and the cell resistance excluding the membrane resistance (see Fig. 2).

First, a reference Nafion® 115 membrane is used. As diffusion coefficients of vanadium ions for a Nafion® 115 membrane are available in the literature, this information is utilized to estimate other cell system parameters, such as rate constants at the electrodes, the formal potential, and the cell resistance excluding the membrane resistance in the batch cell model. Next, the systems approach shows that diffusion coefficients of vanadium ions for other membranes can also be estimated based on the parameters estimated using the Nafion® 115 system. By using this concept, four vanadium ions' diffusion coefficients of a Nafion® XL membrane, which are not available in the literature, have been estimated. Once the parameters have been obtained, one can use the kinetic and transport parameters for simulating redox battery systems as well. The systems approach can be used to update the transport and kinetic parameters or any degradation inputs of redox batteries within a very short span of time during battery operation. Any mismatch between model and data over cycles of operation can be resolved with the updated parameters, and the control of the redox batteries with precise predictions based on the proposed
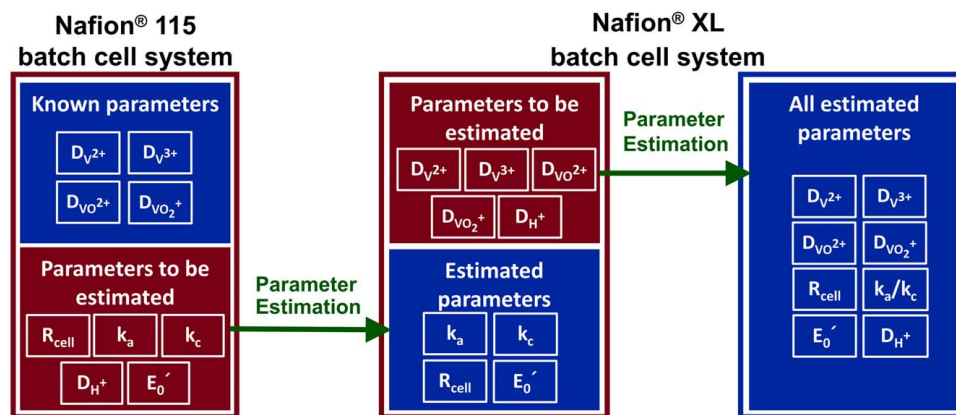
Fig. 2 Parameter estimation of the batch cell system with charging/discharging curves at different C-rates. We show a way of estimating all parameters in a model, which can help analyze and study the performance of the cell system.
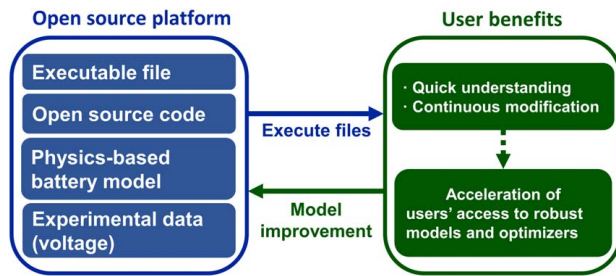
Fig. 3 Open source platfrom and user benefit. Different models and optimizers describing the same systems produce different estimated parameters. On the open source platform, users can improve the model through continuous modification and easy access, and this accelerates to identify proper and robust models and optimizers for redox battery systems.

work might lead to longer battery life and lower battery cost. While an ideal situation in simulations of the physics-based battery models is to obtain proper parameters from independent experiments, many of the experiments require either physical destruction of the battery or the sophisticated experimental setup [15–17]. For example, dialysis cell, pumps, and measuring cylinders are utilized to investigate diffusion coefficients of ions through a membrane in an RFB experimental setup [18]. Techniques such as linear sweep voltammetry and electrochemical impedance spectroscopy were used to investigate reaction rate information for the kinetic parameters at electrodes [19,20]. Therefore, parameter estimation from a systems approach and experiments is complementary, and the proper implementation of two approaches enhances the accuracy of parameter estimation and quick understanding of the system.

(iii) The last objective is to accelerate people's access to robust models and optimization approaches by providing an open source platform.

In the open source platform, users can utilize the experimental data, models, and codes for parameter estimation of the batch cell system for redox flow batteries at one place (see Fig. 3). For example, even though a systems approach helps users to understand the battery system faster, there are some critical issues with redox flow battery simulations: (a) different models and optimizers describing the same systems provide different values of the estimated parameters and (b) there is a time delay for users to adopt approaches because most of the literature just provide the approaches as a paper. The open source platform will help to arrive at robust modeling and optimization approaches for users by the continuous modification of battery models with detailed physics, additional experimental data, and different optimizers. Also, the platform enables to identify the performance of redox batteries without the need for software installation and a priori programming knowledge. These advantages of the open source platform will help accelerate the spread of redox flow battery systems.

Experimental

Materials. Vanadium (IV) oxide sulfate hydrate (VOSO$_4$·xH$_2$O)[2] and an aqueous sulfuric acid solution (H$_2$SO$_4$)[3] were purchased from Sigma Aldrich and used as received. Nafion® XL [21] and Nafion® 115 [22] membranes were purchased from DuPont and used after pretreatment using distilled deionized water (DDW) and an aqueous sulfuric acid solution at 80 °C for 30 min, respectively. Graphite electrodes[4] were purchased from Saturn Industries.

Instrumentation. The performance of the batch cell was obtained at different C-rates, using a Solartron SI 1287 potentiostat.[5]

The Batch Cell System. The H-cell (Adams and Chittenden Scientific Glass)[6] consists of a positive and a negative chamber, as shown in Fig. 1. A membrane in contact with the electrolytes of the half-cell is located between these two chambers. The volume of the electrolytes at the positive and negative chamber is 10 ml each. Two graphite electrodes with the specific reaction surface (1 cm × 1 cm × 0.1 cm) are vertically placed in the center of each chamber and fixed with the plastic caps of the H-cell. There are rubber gaskets inside these plastic caps, and silicon is attached to the gaps between the electrode and the gasket to prevent oxygen leakages from outside the system.

Preparation of Electrolytes. Sulfuric acid solution (H$_2$SO$_4$, 6.73 ml) was slowly added to 7.5 ml of DDW, and the final volume was adjusted to 30 ml using DDW to prepare 4M sulfuric acid solution (H$_2$SO$_4$). A total of 0.603 g of vanadium (IV) oxide sulfate hydrate (VOSO$_4$·xH$_2$O) was added very slowly and stirred at 60 °C for 1 h. The hydration of the vanadium oxide sulfate (VOSO$_4$) was determined by Karl Fischer titration using a Mettler Toledo C20 Coulometric KF Titrator with a DO308 oven attachment [23]. The instrument was located inside a dry room, where the dew point is maintained at −64 °F. Karl Fisher showed that two water molecules were hydrated to one vanadium oxide sulfate (VOSO$_4$·2H$_2$O), and the molecular weight (201.042 g/mol) was calculated based on the indication. Thirty milliliters of 0.1 M vanadium (IV) oxide sulfate (VOSO$_4$) in an aqueous 4M sulfuric acid solution (H$_2$SO$_4$) was prepared. Next, 10 ml of 0.1M vanadium (IV) oxide sulfate (VOSO$_4$) in an aqueous 4M sulfuric acid solution (H$_2$SO$_4$) was added to the positive and negative chambers. The batch cell system was slowly charged at the C/20 rate to convert VO^{2+} to V^{3+} at the anode and VO^{2+} to VO$_2^+$ at the cathode. When the upper limit voltage of 1.7 V was exceeded, the charge was set to be terminated, and 93.9% V^{3+}/6.1% VO^{2+} electrolytes at the negative chamber were achieved by the coulombic calculation. After that, VO^{2+}/VO$_2^+$ electrolytes at the positive chamber were drained and refilled with a new 10 ml of 0.1 M VO^{2+} in 4M sulfuric acid solution (H$_2$SO$_4$).

Cell Operation. Both Nafion® 115 and Nafion® XL systems are operated at low C-rates (∼C/30). In an ideal situation, a C-rate of 1C means the applied current when the battery is charged for one hour. For batch cell operation, 1C was calculated by a mass balance equation given below:

$$1C = \frac{F \cdot C_{VOSO_4} \cdot V_r}{1 \text{ h}} \qquad (1.M)$$

where F is the Faraday constant (=26,801 Ah/mol), C_{VOSO4} is the concentration of vanadium (IV) oxide sulfate (=0.1 mol/L), and V_r presents the volume of electrolytes (=10 ml). Therefore, 1C was derived as 26.8 mA, and C/20 and C/30 were calculated as 1.34 mA, 0.89 mA, respectively. For the Nafion® 115 system, a typical CC-CV profile (CC, constant current; CV, constant voltage) was applied (maximum voltage: 1.7 V). Once the batch cell voltage reached 1.7 V, it was charged with the CV until the applied current is saturated. In other words, CV charging is continued until the exponentially decaying applied current stopped decreasing. For discharging, a CC profile was applied. The CC-CV profile was used to analyze the cell system's performance at different C-rates (C/20 and C/30), making the cell to reach the full capacity. The coulombic efficiency of the Nafion® 115 system is 0.73 at C/30 and 0.81 at C/20 (see *experimental data in*

---

[2]http://www.sigmaaldrich.com/catalog/product/aldrich/233706?lang=en®ion=US
[3]http://www.sigmaaldrich.com/catalog/product/aldrich/339741?lang=en®ion=US
[4]http://poco.com/MaterialsandServices/Graphite.aspx

[5]http://www.ameteksi.com/products/potentiostats/single-channel/12xx-series
[6]http://www.adamschittenden.com/index.php

Figs. 7 and 10). It shows that the higher current rates give the higher coulombic efficiency [24]. For the Nafion® XL cell system, a CC profile was applied to the batch cell system during the charging and discharging processes. The temperature of the H-cell was maintained at 25 °C in a Tenney Environmental Chamber.[7] The gas washer, which was filled with water and connected to the argon line and cell system, minimizes evaporation of electrolytes. During the charging and discharging process, a magnetic stirrer was used to make uniform concentrations of the electrolyte in the positive and negative chambers.

Model Formulation

Various zero-dimensional VRFB models accounting for ion transport phenomena, such as diffusion, migration, and convection, have been developed. In this section, several important zero-dimensional models are validated, using voltage outputs obtained from the batch cell systems equipped with a Nafion® 115 membrane at C/30. First, the diffusion model for a batch cell system demonstrated by Tang et al. is validated [4]. In this diffusion model, the proton transport is removed from governing equations, and the formal potential is used, which combines a standard potential, proton concentration, and ions activity coefficients. Second, the concept of unidirectional ions migration and convection with the same direction of ions diffusion, which was proposed by Boettcher et al. [6], is added to the diffusion model and validated. Third, the antidirectional ions flux is added to the unidirection model and validated. The zero-dimensional model including both unidirectional and antidirectional ion's migration and convection was proposed by Pugach et al. [7]. Finally, the proton concentration is separated from the formal potential, and its transport is added to the full-direction model to formulate an adequate zero-dimensional physics-based model for a systems approach. Ideally, parameters should be estimated from one set of data, and the same set of estimating parameters is used to fit another set of data. However, if the formal potential includes the proton concentration, the formal potential should be estimated for every other C-rate because the proton concentration depends on the applied C-rates. This is not an efficient system approach.

In the model formulation process, simultaneous estimation of multiple parameters, called a systems approach, has been carried out using experimental voltage profiles of charging and discharging protocols for the first cycle (CC-CV charging and CC discharging at C/30). The model parameters are fitted with the experimental data to estimate their values using mathematical optimization techniques. 200 (=N) data points for charge and discharge voltage were collected at regular time intervals. The optimization routine finds the optimal values for which the objective function (as given in Eq. (2.M)) subject to the model equations, initial conditions, and bounds for the parameters is minimized. By using realistic values of these parameters as initial guesses, the model can be simulated to predict the values of voltage at certain time intervals. The final estimated parameters are obtained by solving an optimization problem where the sum of squares of the differences in the voltage outputs between the model and the experiment divided by the total number of experimental data points (known as the mean square error (MSE)) for the first cycle (charging and discharging) of the system is minimized, and unknown parameters are used as decision variables [25]. The objective function of the optimization approach can be expressed as follows [26]:

$$\text{Min} \quad \frac{1}{N - n_p} \sum_{j=1}^{N} [V_{exp,j} - V_{model,j}(\mathbf{p})]^2 \tag{2.M}$$

$$\text{s.t.} \quad \mathbf{p}^L \leq \mathbf{p} \leq \mathbf{p}^U$$

where N is the total number of experimental data points for charging and discharging, n_p is the number of estimating parameters, $V_{exp,j}$ and $V_{model,j}(\mathbf{p})$ indicate the experimental and model predicted voltage value of the batch cell for the jth data point, $\mathbf{p}$ is the vector of the estimating parameters, and $\mathbf{p}^L$ and $\mathbf{p}^U$ represent the lower and upper bounds for the vector of the estimating parameters ($\mathbf{p}$). The trial-and-error method has been utilized to obtain initial guesses and lower/upper bounds in this optimization problem [27]. Initial guesses were set up based on the physical characteristics of the batch system, and lower and upper bounds were adjusted based on the initial guesses (up to 20% from initial guesses for most cases) to obtain converged values of the unknown parameters and identify minimized MSE. Analysis and studies of simulations and optimizations in this work were carried out on a workstation with dual 8-core, 3.10 GHz Intel Xeon processors, 32.0 GB RAM using the NLPsolve[8] in the optimization package of the MAPLE® software [28].

Model 1: Diffusion Model. The diffusion model includes the crossover of the vanadium ions through the membrane by diffusion and the ions' side reactions in the electrolyte, as shown in Fig. 4 [4]. Once vanadium ions cross the membrane, reactions between two different vanadium ions occur, producing VO^{2+} ions at the positive electrolyte and V^{3+} ions at the negative electrolyte, and this, in turn, causes the capacity loss of the battery [4].

Assumptions. The following assumptions were made in the diffusion model for the batch cell system: (i) side reactions between two different vanadium ions, due to the crossover of ions through the membrane, occur immediately when the vanadium ions cross the membrane [12]; (ii) since the gas washer is connected to the batch cell system to minimize evaporation of the electrolyte, evaporation of the electrolyte is ignored in the model; (iii) Faraday's law of electrolysis has been assumed to estimate the rate of reactions of vanadium ions at the cathode and anode; (iv) hydrogen and oxygen that evolve at the electrode during charging and discharging are ignored [10,11]; (v) no side reactions take place between other
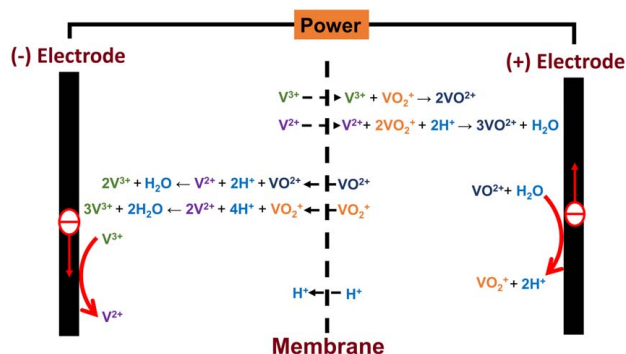
Fig. 4 Side reactions caused by the crossover of vanadium ions through the membrane during charging. One mole of V^{2+}, which moves across the membrane from the negative electrolyte, reacts with two moles of VO_2^+ in the positive electrolytes producing three moles of VO^{2+}. One mole of V^{3+} crossover from the negative electrolyte causes a chemical reaction with one mole of VO_2^+ producing two moles of VO^{2+} in the positive electrolyte. Similarly, in the negative electrolyte, two moles of V^{3+} are produced by a chemical reaction between one mole of V^{2+} and one mole of VO^{2+}, which moves from the positive electrolyte, and three moles of V^{3+} are produced by a chemical reaction between two moles of V^{2+} and one mole of VO_2^+, which moves from the positive electrolyte.

vanadium ions inside the membrane; (vi) the sulfuric acid (H_2SO_4) completely dissociates into protons and sulfate ions (SO_4^{2-}); and (vii) activity coefficients of vanadium ionic species are not equal to 1, and the proton concentration is not accurately known due to several ionic equilibria in the electrolytes [4].

Governing Equations. Accumulation, generation, and diffusion terms of Eqs. (1)–(4) (or (1′)–(4′)) and (5)–(8) (or (5′)–(8′)) in Tables 2 and 3 are used in the diffusion model [4,6]. Tables 2 and 3 include dynamics of concentrations for vanadium ions during charging and discharging, respectively. In the diffusion model, the only difference between governing equations of charging and discharging is the direction of the applied current because the model does not include migration and convection terms. In Tables 2 and 3, mass balance equations, consisting of the rate of accumulation of ions, the rate of ions entering the opposite chamber, the rate of ions flowing out from their own chamber, and the rate of loss or generation of ions, were established for vanadium ions. For example, the rate of accumulation of each vanadium ion species (V^{2+}, V^{3+}, VO^{2+}, and VO_2^+) is the sum of the rate of production of the vanadium ions by side reactions, the rate of outflow into the opposite chamber, and the rate of generation or loss at the electrode by the electrochemical reactions [29].

Additional Equations. Equations (9-1), (10-1), and (11) are used in the diffusion model in Table 4. The cell voltage, the open circuit voltage, and the overpotential are used in the model [3,4,6]. Also, kinetics at the positive and negative electrode is added to the original diffusion model to study more details of the system. The cell voltage is given by Eq. (9-1) [4], and the open circuit voltage is expressed as Eq. (10-1). In the open circuit voltage, the formal potential is used, extracting activity coefficients and proton concentrations from the logarithmic term, following the assumption (vii) [4]. The overpotential at the positive and negative electrodes, including the activation barrier, is calculated as given in Eq. (11), and a charge transfer coefficient of 0.5 is applied to the overpotential [3]. All relevant variables and parameters, which were used to model and simulate the batch system, are listed in Tables 5 and 6, respectively.

Parameter Estimation. There are four parameters to be estimated: the rate constants at the positive and negative electrodes, the cell resistance, and the formal potential. For the best performance of the optimization problem, the rate constants are expressed in term of an exponential function ($k_c = e^{-A}$ and $k_c = e^{-B}$), and indices (A and B) of the exponential function are used as optimizing variables because the original parameters of the rate constants are too small ($\sim 10^{-9}$) to identify properly.

- *Initial guesses*: Initial guesses of parameters are determined within physically reasonable ranges of the VRBC systems. For example, the kinetic constants at electrodes for redox batteries are known to be of the order of 10^{-6} to 10^{-9} [3,12]. The formal potential is known as the value of 1.4 V for 2M vanadium ions in 5M sulfate electrolytes at 50% state of charge [4]. The value of the total resistance of the batch cell is not reported, but its initial guess is determined by fitting with the experimental data based on the initial guesses of other parameters. The initial guesses for the rate constants at the positive and negative electrodes, the formal potential, and the cell resistance were 1.02×10^{-6} m/s, 1.37×10^{-6} m/s, 1.4 V, and 2 Ω, respectively.
- *Lower and upper bounds*: The lower and upper bounds for rate constants at the positive and negative electrodes were 2.50×10^{-6} to 4.04×10^{-6} m/s and 3.56×10^{-7} to 5.29×10^{-6} m/s, respectively. In this case, a range of $\pm 20\%$ from the initial guesses applies to the scaled exponential values (A and B). The bounds for the formal potential were given as 1.26–1.54 V. The lower bound was set up to a standard potential (=1.26 V) for reactions at the positive and negative electrodes in the VRBC system, and the upper bound was determined to

be in the range of +10% from the initial guess. The lower and upper bounds for the cell resistance were 0 and 5 Ω, respectively. The bounds of the batch cell resistance were adjusted to broader ranges to precisely investigate the optimized values because physically meaningful values were not available.

- *Results*: The converged parameters for rate constants at the positive and negative electrodes, the formal potential, and the cell resistance are 2.05×10^{-6} m/s, 4.23×10^{-7} m/s, 1.43 V, and 5 Ω. The minimized MSE was 1.72 mV. The comparison of voltage profiles between model outputs and experimental data is shown in Fig. 7(a). The results indicate that there is a significant discrepancy between the model outputs and the experimental data. Both charging and discharging predictions from model outputs have longer profiles than the experimental data. Addition of more detailed physics and ions transport is required.

Model 2: Diffusion Model + Unidirectional Migration and Convection. The concepts of unidirectional vanadium ions' migration and electroconvection are added to the diffusion model and validated. In the VRFB system, convection effects consist of the hydraulic-osmotic and the electro-osmotic convection [12,13]. The hydraulic-osmotic convection occurs due to water osmosis by the half-cell pressure gradient. This effect causes the crossover of water along with ions through the membrane due to viscous interactions between fluid and charge carriers. In the electro-osmotic convection, ions diffusion and migration lead to a half-cell osmotic gradient, and the water movement due to this osmotic gradient carries the ions again [12,13]. For the hydraulic-osmotic convection, when the volumetric flow of the system is static, the half-cell pressure gradient becomes negligible because the half-cell gradient is proportional to the volumetric flow of the system [12]. In the VRBC system, therefore, the hydraulic-osmotic effect can be negligible due to static electrolytes, and only the electro-osmotic effect is considered [30]. In a real VRBC system, both migration and electro-osmotic convection are applied from the positive to the negative electrolyte during charging and from the negative to the positive during discharging. According to the unidirection zero-dimensional model proposed by Boettcher et al. [6], however, it is not possible for migration and convection effects to have the anti-directional flux to counter the diffusion flux since there are no ion sources from the opposite compartment [6].

Therefore, the unidirection model includes only VO^{2+} and VO_2^+ ions' migration and convection effects from the positive to negative electrolyte during charging and only V^{2+} and V^{3+} ions' migration and convection effects from the negative to the positive electrolyte during discharging, as shown in Fig. 5 [6].

Assumptions. In addition to the assumptions of the diffusion model, one more assumption is added, i.e., assumption (viii). The membrane conductivity is constant during charging and discharging.

Equations. For governing equations, Eqs. (1)–(4) and (5)–(8) in Tables 2 and 3 are used. Unidirectional migration and electro-osmotic convection effects have been added to the diffusion model [3,6,12,30]. For additional equations, Eqs. (9-2), (10-1), and (11)–(13) are used [3,4,6,30]. The cell system's ohmic loss of the diffusion model is divided into ohmic losses associated with the membrane resistance and the cell system resistance excluding the membrane resistance, as shown in Eq. (9-2). The potential gradient and the convection velocity across the membrane can be expressed as Eqs. (12) and (13), respectively [3,4,6,30].

Parameter Estimation. There are five parameters to be estimated; rate constants at the positive and negative electrodes, the cell resistance excluding the membrane resistance, the formal potential, and the membrane conductivity. The membrane

Table 2 Governing equations (charging process)

Accum.	= Gen.	+ In −out (diffusion term)	(Migration and electro-osmotic convection term) antidirectional term	No.
Unidirectional model				
$V_r \dfrac{dC_{V^{2+}}(t)}{dt}$	$= +\dfrac{i_{app}}{F}$	$-(D_{V^{2+}}C_{V^{2+}}(t) + 2D_{VO_2^+}C_{VO_2^+}(t) + D_{VO^{2+}}C_{VO^{2+}}(t))\dfrac{A_m}{d_m}$	$-2(D_{VO^{2+}}C_{VO^{2+}}(t) + D_{VO_2^+}C_{VO_2^+}(t))\dfrac{F}{RT}A_m\nabla\phi - (C_{VO^{2+}}(t) + 2C_{VO_2^+}(t))v_m A_m$	(1)
$V_r \dfrac{dC_{V^{3+}}(t)}{dt}$	$= -\dfrac{i_{app}}{F}$	$-(D_{V^{3+}}C_{V^{3+}}(t) - 3D_{VO_2^+}C_{VO_2^+}(t) - 2D_{VO^{2+}}C_{VO^{2+}}(t))\dfrac{A_m}{d_m}$	$+(4D_{VO^{2+}}C_{VO^{2+}}(t) + 3D_{VO_2^+}C_{VO_2^+}(t))\dfrac{F}{RT}A_m\nabla\phi + (2C_{VO^{2+}}(t) + 3C_{VO_2^+}(t))v_m A_m$	(2)
$V_r \dfrac{dC_{VO^{2+}}(t)}{dt}$	$= -\dfrac{i_{app}}{F}$	$-(D_{VO^{2+}}C_{VO^{2+}}(t) - 3D_{V^{2+}}C_{V^{2+}}(t) - 2D_{V^{3+}}C_{V^{3+}}(t))\dfrac{A_m}{d_m}$	$-2D_{VO^{2+}}C_{VO^{2+}}(t)\dfrac{F}{RT}A_m\nabla\phi - 2v_m A_m C_{VO^{2+}}(t)$	(3)
$V_r \dfrac{dC_{VO_2^+}(t)}{dt}$	$= +\dfrac{i_{app}}{F}$	$-(D_{VO_2^+}C_{VO_2^+}(t) + 2D_{V^{2+}}C_{V^{2+}}(t) + D_{V^{3+}}C_{V^{3+}}(t))\dfrac{A_m}{d_m}$	$-D_{VO_2^+}C_{VO_2^+}(t)\dfrac{F}{RT}A_m\nabla\phi - v_m A_m C_{VO_2^+}(t)$	(4)
Full-directional model				
$V_r \dfrac{dC_{V^{2+}}(t)}{dt}$	$= +\dfrac{i_{app}}{F}$	$-(D_{V^{2+}}C_{V^{2+}}(t) + 2D_{VO_2^+}C_{VO_2^+}(t) + D_{VO^{2+}}C_{VO^{2+}}(t))\dfrac{A_m}{d_m}$	$-2(D_{VO^{2+}}C_{VO^{2+}}(t) + D_{VO_2^+}C_{VO_2^+}(t) - D_{V^{2+}}C_{V^{2+}}(t))\dfrac{F}{RT}A_{mem}\nabla\phi - (C_{VO^{2+}}(t) + 2C_{VO_2^+}(t) - C_{V^{2+}}(t))v_m A_m$	(1′)
$V_r \dfrac{dC_{V^{3+}}(t)}{dt}$	$= -\dfrac{i_{app}}{F}$	$-(D_{V^{3+}}C_{V^{3+}}(t) - 3D_{VO_2^+}C_{VO_2^+}(t) - 2D_{VO^{2+}}C_{VO^{2+}}(t))\dfrac{A_m}{d_m}$	$+(4D_{VO^{2+}}C_{VO^{2+}}(t) + 3D_{VO_2^+}C_{VO_2^+}(t) + 3D_{V^{3+}}C_{V^{3+}}(t))\dfrac{F}{RT}A_{mem}\nabla\phi + (2C_{VO^{2+}}(t) + 3C_{VO_2^+}(t) + C_{V^{3+}}(t))v_m A_m$	(2′)
$V_r \dfrac{dC_{VO^{2+}}(t)}{dt}$	$= -\dfrac{i_{app}}{F}$	$-(D_{VO^{2+}}C_{VO^{2+}}(t) - 3D_{V^{2+}}C_{V^{2+}}(t) - 2D_{V^{3+}}C_{V^{3+}}(t))\dfrac{A_m}{d_m}$	$-2(D_{VO^{2+}}C_{VO^{2+}}(t) + 3D_{V^{2+}}C_{V^{2+}}(t) + 3D_{V^{3+}}C_{V^{3+}}(t))\dfrac{F}{RT}A_{mem}\nabla\phi - (C_{VO^{2+}}(t) + 3C_{V^{2+}}(t) + 2C_{V^{3+}}(t))v_m A_m$	(3′)
$V_r \dfrac{dC_{VO_2^+}(t)}{dt}$	$= +\dfrac{i_{app}}{F}$	$-(D_{VO_2^+}C_{VO_2^+}(t) + 2D_{V^{2+}}C_{V^{2+}}(t) + D_{V^{3+}}C_{V^{3+}}(t))\dfrac{A_m}{d_m}$	$-(D_{VO_2^+}C_{VO_2^+}(t) - 4D_{V^{2+}}C_{V^{2+}}(t) - 3D_{V^{3+}}C_{V^{3+}}(t))\dfrac{F}{RT}A_{mem}\nabla\phi - (C_{VO_2^+}(t) - 2C_{V^{2+}}(t) - C_{V^{3+}}(t))v_m A_m$	(4′)

Note: Accum., accumulation; Gen., generation.

Table 3   Governing equations (discharging process)

Accum.	= Gen.	+In −out (diffusion terms)	(Migration and electro-osmotic convection terms)	No.
Unidirectional model				
$V_r \dfrac{dC_{V^{2+}}(t)}{dt}$	$= -\dfrac{i_{app}}{F}$	$-(D_{V^{2+}} C_{V^{2+}}(t) + 2D_{VO_2^+} C_{VO_2^+}(t) + D_{VO^{2+}} C_{VO^{2+}}(t))\dfrac{A_m}{d_m}$	$-2D_{V^{2+}} C_{V^{2+}}(t) \dfrac{F}{RT} \dfrac{\Delta\phi(t)}{d_m} A_m - v_m C_{V^{2+}}(t) A_m$	(5)
$V_r \dfrac{dC_{V^{3+}}(t)}{dt}$	$= +\dfrac{i_{app}}{F}$	$-(D_{V^{3+}} C_{V^{3+}}(t) - 3D_{VO_2^+} C_{VO_2^+}(t) - 2D_{VO^{2+}} C_{VO^{2+}}(t))\dfrac{A_m}{d_m}$	$-3D_{V^{3+}} C_{V^{3+}}(t) \dfrac{F}{RT} \dfrac{\Delta\phi(t)}{d_m} A_m - v_m C_{V^{3+}}(t) A_m$	(6)
$V_r \dfrac{dC_{VO^{2+}}(t)}{dt}$	$= +\dfrac{i_{app}}{F}$	$-(D_{VO^{2+}} C_{VO^{2+}}(t) - 3D_{V^{2+}} C_{V^{2+}}(t) - 2D_{V^{3+}} C_{V^{3+}}(t))\dfrac{A_m}{d_m}$	$+6(D_{V^{2+}} C_{V^{2+}}(t) + D_{V^{3+}} C_{V^{3+}}(t))\dfrac{F}{RT} \dfrac{\Delta\phi(t)}{d_m} A_m + (3C_{V^{2+}}(t) + 2C_{V^{3+}}(t)) v_m A_m$	(7)
$V_r \dfrac{dC_{VO_2^+}(t)}{dt}$	$= -\dfrac{i_{app}}{F}$	$-(D_{VO_2^+} C_{VO_2^+}(t) + 2D_{V^{2+}} C_{V^{2+}}(t) + D_{V^{3+}} C_{V^{3+}}(t))\dfrac{A_m}{d_m}$	$-(4D_{V^{2+}} C_{V^{2+}}(t) + 3D_{V^{3+}} C_{V^{3+}}(t))\dfrac{F}{RT} \dfrac{\Delta\phi(t)}{d_m} A_m - (2C_{V^{2+}}(t) + C_{V^{3+}}(t)) v_m A_m$	(8)
Full-directional model				
$V_r \dfrac{dC_{V^{2+}}(t)}{dt}$	$= -\dfrac{i_{app}}{F}$	$-(D_{V^{2+}} C_{V^{2+}}(t) + 2D_{VO_2^+} C_{VO_2^+}(t) + D_{VO^{2+}} C_{VO^{2+}}(t))\dfrac{A_m}{d_m}$	$-2(D_{V^{2+}} C_{V^{2+}}(t) - D_{VO^{2+}} C_{VO^{2+}}(t) - D_{VO_2^+} C_{VO_2^+}(t))\dfrac{F}{RT} A_m \nabla\phi - (C_{V^{2+}}(t) - C_{VO^{2+}}(t) - 2C_{VO_2^+}(t)) v_m A_m$	(5′)
$V_r \dfrac{dC_{V^{3+}}(t)}{dt}$	$= +\dfrac{i_{app}}{F}$	$-(D_{V^{3+}} C_{V^{3+}}(t) - 3D_{VO_2^+} C_{VO_2^+}(t) - 2D_{VO^{2+}} C_{VO^{2+}}(t))\dfrac{A_m}{d_m}$	$-(3D_{V^{3+}} C_{V^{3+}}(t) + 4D_{VO^{2+}} C_{VO^{2+}}(t) + 3D_{VO_2^+} C_{VO_2^+}(t))\dfrac{F}{RT} A_m \nabla\phi - (C_{V^{3+}}(t) + 2C_{VO^{2+}}(t) + 3C_{VO_2^+}(t)) v_m A_m$	(6′)
$V_r \dfrac{dC_{VO^{2+}}(t)}{dt}$	$= +\dfrac{i_{app}}{F}$	$-(D_{VO^{2+}} C_{VO^{2+}}(t) - 3D_{V^{2+}} C_{V^{2+}}(t) - 2D_{V^{3+}} C_{V^{3+}}(t))\dfrac{A_m}{d_m}$	$+2(3D_{V^{2+}} C_{V^{2+}}(t) + 3D_{V^{3+}} C_{V^{3+}}(t) + D_{VO^{2+}} C_{VO^{2+}}(t))\dfrac{F}{RT} A_m \nabla\phi + (3C_{V^{2+}}(t) + 2C_{V^{3+}}(t) + C_{VO^{2+}}(t)) v_m A_m$	(7′)
$V_r \dfrac{dC_{VO_2^+}(t)}{dt}$	$= -\dfrac{i_{app}}{F}$	$-(D_{VO_2^+} C_{VO_2^+}(t) + 2D_{V^{2+}} C_{V^{2+}}(t) + D_{V^{3+}} C_{V^{3+}}(t))\dfrac{A_m}{d_m}$	$-(4D_{V^{2+}} C_{V^{2+}}(t) + 3D_{V^{3+}} C_{V^{3+}}(t) - D_{VO_2^+} C_{VO_2^+}(t))\dfrac{F}{RT} A_m \nabla\phi - (2C_{V^{2+}}(t) + C_{V^{3+}}(t) - C_{VO_2^+}(t)) v_m A_m$	(8′)

Note: Accum., accumulation; Gen., generation.

Table 4 Other equations of all-vanadium redox batch batteries

	No.

$$E_{cell}(t) = E_{cell}^{rev}(t) - i_{app}R_{cell,total} + \eta_2(t) - \eta_1(t)$$

(9-1)

$$E_{cell}(t) = E_{cell}^{rev}(t) + i_{app}R_{cell-mem} + i_{app}\frac{d_m}{A_m\sigma_m} + \eta_2(t) - \eta_1(t)$$

(9-2)

$$E_{cell}^{rev}(t) = E_0' + \frac{RT}{F}\ln\left(\frac{C_{V^{2+}}(t)C_{VO_2^+}(t)}{C_{V^{3+}}(t)C_{VO^{2+}}(t)}\right)$$

(10-1)

$$E_{cell}^{rev}(t) = E_0' + \frac{RT}{F}\ln\left(\frac{C_{V^{2+}}(t)\,C_{VO_2^+}(t)\,C_{H_p^+}(t)^2}{C_{V^{3+}}(t)\,C_{VO^{2+}}(t)}\right)$$

(10-2)

$$\eta_1(t) = -\frac{2RT}{F}\arcsin\left(\frac{i_{app}}{2Fk_a\sqrt{C_{V^{3+}}(t)\,C_{V^{2+}}(t)}}\right), \quad \eta_2(t) = \frac{2RT}{F}\arcsin\left(\frac{i_{app}}{2Fk_c\sqrt{C_{VO^{2+}}(t)\,C_{VO_2^+}(t)}}\right)$$

(11)

$$v_{mem} = \frac{\kappa c_f F}{u_w A_m \sigma_m}i_{app}$$

(12)

$$\nabla\phi = \frac{i_{app}}{A_m\sigma_m}$$

(13)

$$\sigma_m = \frac{F^2}{RT}\sum_i z_i^2 C_i(t)D_i \approx \frac{F^2}{RT}(C_{H_p^+}(t) + C_{H_n^+}(t))D_{H^+}$$

(14)

Table 5 Variables of all-vanadium redox batch cell systems

Symbol	Variable	Units
$C_{V^{2+}}(t)$	Concentration of vanadium (II)	mol m^{-3}
$C_{V^{3+}}(t)$	Concentration of vanadium (III)	mol m^{-3}
$C_{VO^{2+}}(t)$	Concentration of vanadium (IV)	mol m^{-3}
$C_{VO_2^+}(t)$	Concentration of vanadium (V)	mol m^{-3}
$C_{H_p^+}(t)$	Concentration of proton in positive electrolytes	mol m^{-3}
$C_{H_n^+}(t)$	Concentration of proton in negative electrolytes	mol m^{-3}
$E_{cell}(t)$	Cell voltage	V
$E_{cell}^{rev}(t)$	Open circuit voltage	V
$\eta_1(t)$	Overpotential at anode	V
$\eta_2(t)$	Overpotential at cathode	V

resistance can be quantified by dividing the thickness of the membrane by the membrane area and conductivity (see Eq. (9-2)).

- *Initial guesses*: The same initial guesses are applied to the same parameters used in the diffusion model. The initial guess for the additional parameter, i.e., the membrane conductivity, is determined at a value of 10 S/m based on the known physical range of the Nafion® 115 membrane conductivity within 5 and 30 S/m [7,13,31].
- *Lower and upper bounds*: The same bounds are used for the same parameters of the diffusion model. The bounds for the membrane conductivity were given as 0–20 S/m to find the optimal value within a physically meaningful range, and the lower and upper bounds for the cell resistance excluding the membrane resistance were 0–5 Ω, respectively.

- *Results*: The converged parameters for rate constants at the positive and negative electrodes, the cell resistance excluding the membrane resistance, the formal potential, and the membrane conductivity are 8.75×10^{-7} m/s, 1.36×10^{-6} m/s, 5 Ω, 1.45 V, and 4.84 S/m, respectively. Also, the minimized MSE was 0.46 mV. The comparison of voltage profiles between model outputs and experimental data is presented, as shown in Fig. 7(*b*). The result shows that the end part of the charging profile between model outputs and the experimental data is not matched well. The longer charging profile is predicted from model outputs compared with the experimental data. Therefore, more accurate zero-dimesional models are required, adding detailed physics or ion transport.

Model 3: Diffusion Model + Full-Directional Migration and Convection. In this section, antidirectional migration and electroosmotic convection for diffusion are added to the unidirection model in the previous section. The zero-dimentional model, which includes both antidirectional and unidirectional migration and convection, was proposed by Pugach et al. [7].

This model adopts analytical solutions for ions' migration and convection [13] and uses the formal potential to calculate the open circuit potential. When vanadium ions cross the membrane, the ions face the potential gradient, which slows down or increases the total ion flux, as described in Fig. 6. The migration and electroosmotic convection effects occur from the positive side to the negative side during charging, which is in the same direction to the diffusion flux of VO^{2+} and VO$_2^+$ and the opposite direction to the diffusion flux of V^{2+} and V^{3+}. During discharging, the migration and electro-osmotic convection effects occur from the negative

Table 6 Parameters of all-vanadium redox batch cell system used in simulations

Symbol	Parameter	Values	Units
Geometrical parameters			
d_m	Thickness of membrane—Nafion® 115	127×10^{-6}	m
	Thickness of membrane—Nafion® XL	27.5×10^{-6}	
A_m	Cross-sectional area of the membrane	1.77×10^{-4}	m^2
A_e	Surface area of the electrode for reaction	2.3×10^{-4}	m^2
V_r	Volume of electrolyte	10^{-5}	m^3
T	Temperature	298	K
Operational parameters			
i_{app}	Applied current	C/20: 1.34×10^{-3}	A
		C/30: 0.89×10^{-3}	
j_{app}	Current density	C/20: 5.83	A m^{-2}
		C/20: 3.87	
Parameters collected from the literature			
F	Faraday constant	96,485.34	s A mol^{-1}
R	Ideal gas constant	8.314	J K^{-1} mol^{-1}
κ	Electrokinetic permeability of membrane	1.95×10^{-19}	m^2
c_f	Concentration of fixed charge in membrane	1900	mol m^{-3}
u_w	Water viscosity	8.9×10^{-4}	Pa s
$D_{V^{2+}}$	V^{2+} diffusion coefficient of Nafion® 115	0.88×10^{-11}	m^2 s^{-1}
$D_{V^{3+}}$	V^{3+} diffusion coefficient of Nafion® 115	0.32×10^{-11}	m^2 s^{-1}
$D_{VO^{2+}}$	VO^{2+} diffusion coefficient of Nafion® 115	0.68×10^{-11}	m^2 s^{-1}
$D_{VO_2^+}$	VO_2^+ diffusion coefficient of Nafion® 115	0.59×10^{-11}	m^2 s^{-1}
Initial concentration			
$C^0_{V^{2+}}$	Initial concentration of V^{2+} ions	0.001	mol m^{-3}
$C^0_{V^{3+}}$	Initial concentration of V^{3+} ions	93.9	mol m^{-3}
$C^0_{VO^{2+}}$	Initial concentration of VO^{2+} ions	99.999	mol m^{-3}
$C^0_{VO_2^+}$	Initial concentration of VO_2^+ ions	0.001	mol m^{-3}
$C^0_{H^+_p}$	Initial concentration of protons at the positive electrolytes	8000	mol m^{-3}
$C^0_{H^+_n}$	Initial concentration of protons at the negative electrolytes	8000	mol m^{-3}
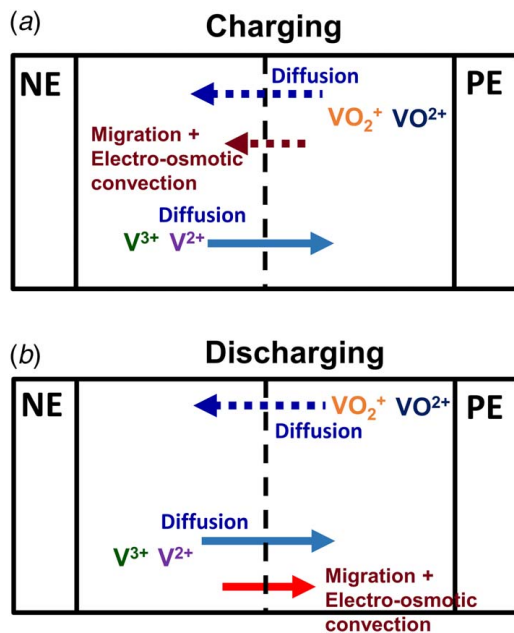
Fig. 5 Crossover of vanadium ions through the membrane in the unidirection model during (a) charging and (b) discharging. PE and NE represent positive and negative electrodes, respectively. A blue dotted arrow indicates VO^{2+}/VO_2^+ diffusion (see the first arrow from the top in (a) charging and (b) discharging), a wine-colored dotted arrow represents VO^{2+}/VO_2^+ migration and electro-osmotic convection (see the second arrow from the top in (a) charging), a sky blue solid arrow shows V^{2+}/V^{3+} diffusion (see the third arrow from the top in (a) charging and the second arrow from the top in (b) discharging), and a red solid arrow represents V^{2+}/V^{3+} migration and electro-osmotic convection (see the third arrow from the top in (b) discharging).

side to the positive side for vanadium ions of the system. In vanadium redox battery systems, when migration and convection are in the opposite direction to diffusion, the diffusion effect is typically larger than the sum of migration and convection effect [12]. In this case, it might be reasonable for a zero-dimensional model to include both unidirectional and antidirectional convection and migration. To ensure that this concept helps to improve the accuracy of the model, the full-direction model is validated.

Assumptions. The same assumptions used in the unidirection model are used.

Equations. For governing equations, Eqs. (1′)–(4′) and (5′)–(8′) in Tables 2 and 3 are used. The same additional Eqs. (9-2), (10-1), (11), (12), and (13) used in the unidirection model are used.

Parameter Estimation. The same parameters used in the unidirection model are estimated, and all initial guesses and bounds are the same as that of the unidirection model.

- *Results*: The converged parameters for the rate constants at the positive and negative electrodes, the cell resistance excluding the membrane resistance, the formal potential, and the membrane conductivity are 1.20×10^{-6} m/s, 1.16×10^{-6} m/s, 2.95 Ω, 1.45 V, and 6.05 S/m, respectively. Also, the minimized MSE was 0.19 mV. The fit of voltage profiles between model outputs and experimental data has a good agreement, as shown in Fig. 7(c). According to the literature, both zero-dimesional uni- and full-direction models for VRFB systems are fitted well with experimental data for a single cycle [6,7]. In the VRBC system at low C-rates, however, only the full-direction model leads to more accurate prediction compared with the unidirection model. One of the possible reasons is that in the VRBC system at low C-rates, capacity loss occurs explicitly even for the first cycle. Adding inaccurate ions transport terms can cause significant
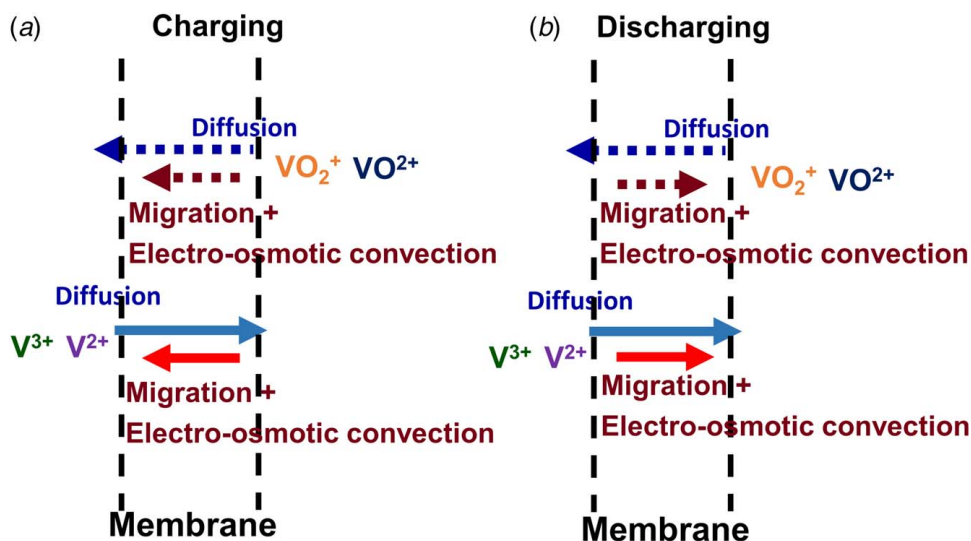
Fig. 6 Crossover of vanadium ions through the membrane by diffusion, migration, and electro-osmotic convection during (a) charging and (b) discharging. A blue dotted arrow indicates VO^{2+}/VO_2^+ diffusion (see the first arrow from the top in (a) charging and (b) discharging), a wine-colored dotted arrow represents VO^{2+}/VO_2^+ migration and electro-osmotic convection (see the second arrow from the top in (a) charging and (b) discharging), a sky blue solid arrow shows V^{2+}/V^{3+} diffusion (see the third arrow from the top in (a) charging and (b) discharging), and a red solid arrow represents V^{2+}/V^{3+} migration and electro-osmotic convection (see the fourth arrow from the top in (a) charging and (b) discharging). The main transport phenomena of the batch system are diffusion, migration, and electro-osmotic convection. The diffusion of vanadium ions through the membrane has the same direction regardless of charging and discharging, and the direction of migration and electro-osmotic convection through the membrane is affected by charging/discharging conditions.

differences between model outputs and experimental data. This can be a good example of showing how the batch cell system at low C-rates, which does not look like a practical system, can contribute to improve the model development, and why the systems approach is essential for the accurate prediction of the battery performance.

Model 4: Diffusion Model + Full-Directional ion Flux + Proton Transport. In the full-direction model, the formal potential was derived by taking the proton concentration and activity coefficients of vanadium ions from the logarithmic term of the open circuit voltage.

In this case, the value of the formal potential needs to be identified or estimated for every other C-rate and different systems including different membranes. This is not an efficient way of utilizing a systems approach. The ideal case is that one set of all estimated parameters obtained from one set of the experimental data should be applied to other sets of the experimental data. For this, the dynamics of proton concentrations is added to the full-direction model. In the previous section, the membrane conductivity was assumed to be constant during the cell operation. However, the membrane conductivity can be approximated by Eq. (14) in Table 4, including the protons' concentration and diffusion coefficient. By doing this, the proton transport effect is added to the full-direction model while keeping the number of estimated parameters same.

Assumptions. The assumption (vii) for the diffusion model need to be modified as follows: (vii) activity coefficients of vanadium ionic species are not equal to 1.

Equations. For governing equations, Eqs. (1′)–(4′), (5′)–(8′), and (15)–(18) in Tables 2, 3, and 7 are used, respectively. For additional equations, Eqs. (9-2), (10-2), and (11)–(14) in Table 4 are used. The logarithmic term of the open circuit voltage, including the proton concentration term, is used as shown in Eq. (10-2), and the membrane conductivity is expressed as Eq. (14).

Parameter Estimation. There are five parameters to be estimated: rate constants at the positive and negative electrodes, the cell resistance excluding the membrane resistance, the formal potential, and the diffusion coefficient of protons. The initial guesses, bounds, and converged parameters are summarized in Table 8, and values in Table 8 were rounded off to the third decimal place.

- *Initial guesses*: Initial guesses for rate constants at the positive and negative electrodes and the cell resistance excluding the membrane resistance are the same with the full-direction model. However, initial guesses of the formal potential and protons' diffusion coefficient are determined as the value of 1.35 V and 1.03×10^{-10} m²/s, respectively. The converged value of the formal potential of the proposed model in this section is expected to be smaller than the converged value from the full-direction model in the previous section since the proton concentration term is taken from the logarithmic term and added back to the logarithmic term of Eq. (10-2). Also, Nafion® membranes typically allow the proton transport 10^2–10^3 times faster than other ions [12,30].

- *Lower and upper bounds*: Bounds for rate constants at the positive and negative electrodes and the cell resistance excluding the membrane resistance are the same as the full-direction model. The bounds for the formal potential were given as 1.26 V–1.49 V. A standard potential was used for the lower bound, and a deviation of +10% from the initial condition was applied to the upper bound. The ±20% ranges of lower and upper bounds for the diffusion coefficient of protons were applied to the scaled exponential values. Therefore, the bounds for the diffusion coefficient of protons were given as 1.03×10^{-11} to 1.02×10^{-9} m²/s.

- *Results*: The converged parameters for rate constants at the positive and negative electrodes, the cell resistance excluding the membrane resistance, the formal potential, and the diffusion coefficient of protons are 1.13×10^{-6} m/s, 1.13×10^{-6} m/s,
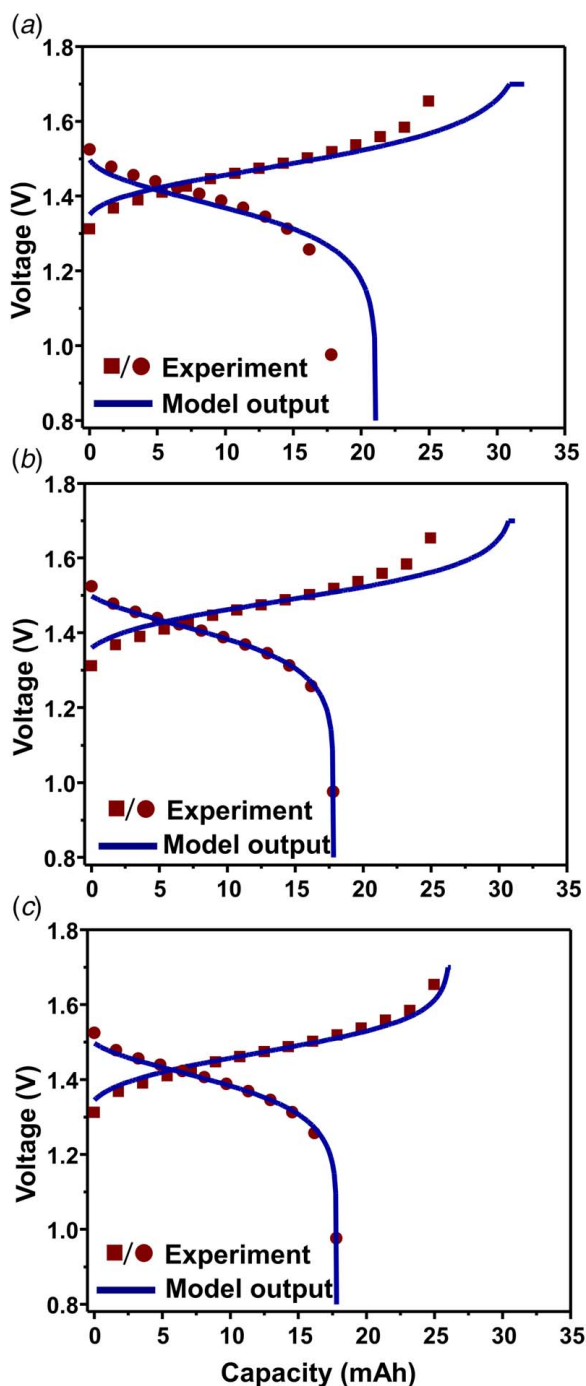
Fig. 7   Model formulation process and comparison of voltage profiles between different model outputs and experimental data from the batch cell system including the Nafion® 115 membrane. Voltage profiles at C/30 (Experimental data: charge (wine color and filled square dots), discharge (wine color and filled circle), and the model (blue straight line). (a) Diffusion model, (b) unidirection model, and (c) full-direction model. Parameters were simultaneously estimated at C/30, minimizing the mean of the sum-of-squared differences between the model and experiment outputs.

2.98 Ω, 1.35 V, and 1×10^{-10} m²/s, respectively. Also, the minimized MSE was 0.22 mV, and a good agreement between model outputs and experimental data is observed, as shown in Fig. 8(a). To study and analyze the effects of ions' transport in the VRBC system, a simple model, which does not include diffusion, migration, and electro-osmotic

convection of vanadium ions through the membrane, is presented as shown in Figs. 8(b), 8(d), and 8(f). There are no mathematical equations describing the crossover of vanadium ions through the membrane in the simple model. So, in the simple model, only Accumulation and Generation terms of Eqs. (1)–(4) (or (1')–(4')) and (5)–(8) (or (5')–(8')) in Tables 2 and 3 are used for charging and discharging, respectively. Except for the governing equations of vanadium ions, the same equations used in the full-direction model including the proton effect are simulated adopting the proton transport (Eqs. (15)–(18) in Table 7), additional equations (Eqs. (9-2), (10-2), (11), (12), and (13) in Table 4) with parameters (Table 6), and estimated parameters (Table 8).

In Figs. 8(a) and 8(b), the charging profile of the VRBC model that includes the effect of diffusion, migration, and convection is found longer than that of the simple model. Partial self-discharge of vanadium ions through the membrane is one of the main reasons for this capacity loss. To study this capacity loss in details, Figs. 8(c)–8(f) describe the comparison of the predicted concentration of vanadium ions for the VRBC system and the simple model. Ideally, V^{2+} ions should be generated only from V^{3+} ions through an electrochemical reaction at the negative electrode during charging (see Fig. 8(d)). In reality, V^{2+} ions are continuously depleted in negative electrolytes due to side reactions with VO^{2+}/VO_2^+ ions and crossover of V^{2+} ions through the membrane (see Fig. 8(c)). Likewise, VO_2^+ ions should be only produced for charging (see Fig. 8(f)), but they are also depleted in the positive electrolyte because of their crossover and side reactions giving rise to VO^{2+} ions (see Fig. 8(e)). The self-discharge of vanadium ions, which happens during charging, causes a slower charging until the cell is achieved at the maximum voltage.

In contrast, this self-discharge leads to faster discharge in shorter discharge time. During discharge, V^{2+} and VO_2^+ ions are depleted due to electrochemical reactions at the negative electrode and their side reactions with other vanadium ions and crossover through the membrane, thereby dropping the concentration of V^{2+} and VO_2^+ ions faster (see Figs. 8(c) and 8(e)). For this reason, the self-discharge of vanadium ions, which happens during discharge, causes a faster discharge until the cell achieves the minimum voltage. Importantly, the VRBC/VRFB system does not produce any inert third compound, such as Li-ion SEI/plating, that can cause irreversible capacity loss [32]. Rather, side reactions in VRBC/VRFB systems are disproportionate reactions, which convert vanadium ions from one oxidation state to another state [4].

- *Sensitivity analysis for the initial guess*: Table 9 describes the sensitivity analysis for the initial guess. The sensitivity analysis was conducted with changes of −10%, −5%, +5%, and 10% from the original initial guess. When one initial guess is changed, the other initial guesses remain at their original value. For the Nafion® 115 system, the optimal value of most parameters is stable for the changes in initial guesses (up to 20%). However, the cell resistance excluding the membrane shows a tendency to be unstable for initial guesses variations.

Systems Approach to Different Membranes

In this section, a systems approach is performed with the Nafion® XL system, using the full-direction model including the proton transport in the previous section. In the Nafion® 115 and Nafion® XL system, some parameters are known a priori, while other parameters are estimated through the parameter estimation approach, as shown in Fig. 2. For example, diffusion coefficients of vanadium ions for other membranes, which have not yet been investigated, are estimated based on the predetermined other parameters in the Nafion® 115 cell system. The Nafion® XL membrane equipped batch cell system has been considered, where diffusion coefficients have not been identified. Therefore, there are total ten parameters to

Table 7 Governing equations for proton transport

Accumulation	= Generation	+ In − out (diffusion terms)	(Migration and electro-osmotic convection terms)	No.
Charge				
$V_r \dfrac{dC_{H_p^+}(t)}{dt}$	$= +\dfrac{2i_{app}}{F}$	$+(D_{H^+}C_{H_n^+}(t) - D_{H^+}C_{H_p^+}(t))\dfrac{A_m}{d_m}$	$-(D_{H^+}C_{H_p^+}(t) + D_{H^+}C_{H_n^+}(t))\dfrac{F}{RT}A_m\nabla\phi - v_m(C_{H_p^+}(t) + C_{H_n^+}(t))A_m$	(15)
$V_r \dfrac{dC_{H_n^+}(t)}{dt}$	$= 0$	$+(-D_{H^+}C_{H_n^+}(t) + D_{H^+}C_{H_p^+}(t))\dfrac{A_m}{d_m}$	$+(D_{H^+}C_{H_p^+}(t) + D_{H^+}C_{H_n^+}(t))\dfrac{F}{RT}A_m\nabla\phi + v_m(C_{H_p^+}(t) + C_{H_n^+}(t))A_m$	(16)
Discharge				
$V_r \dfrac{dC_{H_p^+}(t)}{dt}$	$= -\dfrac{2i_{app}}{F}$	$+(D_{H^+}C_{H_n^+}(t) - D_{H^+}C_{H_p^+}(t))\dfrac{A_m}{d_m}$	$+(D_{H^+}C_{H_p^+}(t) + D_{H^+}C_{H_n^+}(t))\dfrac{F}{RT}A_m\nabla\phi + v_m(C_{H_p^+}(t) + C_{H_n^+}(t))A_m$	(17)
$V_r \dfrac{dC_{H_n^+}(t)}{dt}$	$= 0$	$+(-D_{H^+}C_{H_n^+}(t) + D_{H^+}C_{H_p^+}(t))\dfrac{A_m}{d_m}$	$-(D_{H^+}C_{H_p^+}(t) + D_{H^+}C_{H_n^+}(t))\dfrac{F}{RT}A_m\nabla\phi - v_m(C_{H_p^+}(t) + C_{H_n^+}(t))A_m$	(18)

be estimated: four diffusion coefficients of different vanadium ionic species for Nafion XL, two diffusion coefficients of protons for Nafion® 115 and XL membranes, the cell resistance excluding the membrane resistance, two rate constants at cathode and anode, and the formal potential. While system parameters including the formal potential, the cell resistance excluding the membrane resistance, and two rate constants at electrodes remain the same as obtained for the Nafion® 115 system, other remaining parameters including five diffusion coefficients of the ionic species through the Nafion® XL membrane are estimated through the systems approach. The diffusion coefficients of five ionic species are expressed and scaled in term of exponential functions as well, where the indices appearing to the power of the exponential factor (e) are used as the parameters for optimization.

Assumption and Equations. The same assumptions and equations used in the full-direction model are used.

Parameter Estimation. The same systems approach used in the full-direction model inlcuding the proton transport has been attempted at C/30. There are five parameters to be estimated: five diffusion coefficients of vanadium ions and protons. The initial guesses, bounds, and converged parameters are summarized in Table 8, and values in Table 8 were rounded off to the third decimal place.

- *Initial guesses:* Diffusion coefficients of the Nafion® membrane are known to be in the range of 10^{-11} to 10^{-13} [4,6,12], and the diffusion coefficient of protons is known to be in the scale of 10^{-9} to 10^{-10}. Based on this information, the initial guesses for diffusion coefficients of V^{2+}, V^{3+}, VO^{2+}, VO_2^+, and protons were determined as the value of 1.88×10^{-12} m²/s, 1.88×10^{-12} m²/s, 1.03×10^{-11} m²/s, 5.11×10^{-12} m²/s, and 2.79×10^{-10} m²/s, respectively.
- *Lower and upper bounds*: The range of lower and upper bounds for ions diffusion coefficients was set up using the scaled exponential values with a range of $\pm 20\%$ from the initial guesses. Therefore, the lower and upper bounds for diffusion coefficients of V^{2+}, V^{3+}, VO^{2+}, VO_2^+, and protons were 1.26×10^{-13} to 2.80×10^{-11} m²/s, 1.26×10^{-13} to 2.80×10^{-11} m²/s, 8.2×10^{-13} to 1.29×10^{-10} m²/s, 3.79×10^{-13} to 6.88×10^{-11} m²/s, and 3.09×10^{-11} to 2.52×10^{-9} m²/s, respectively.
- *Results*: The converged values for diffusion coefficients of V^{2+}, V^{3+}, VO^{2+}, VO_2^+, and protons are estimated as 0.88×10^{-12} m²/s, 1.27×10^{-12} m²/s, 1.02×10^{-11} m²/s, 4.67×10^{-12} m²/s, and 1.66×10^{-10} m²/s, respectively. The minimized MSE of the Nafion® XL system is 1.21 mV. Figure 9(a)
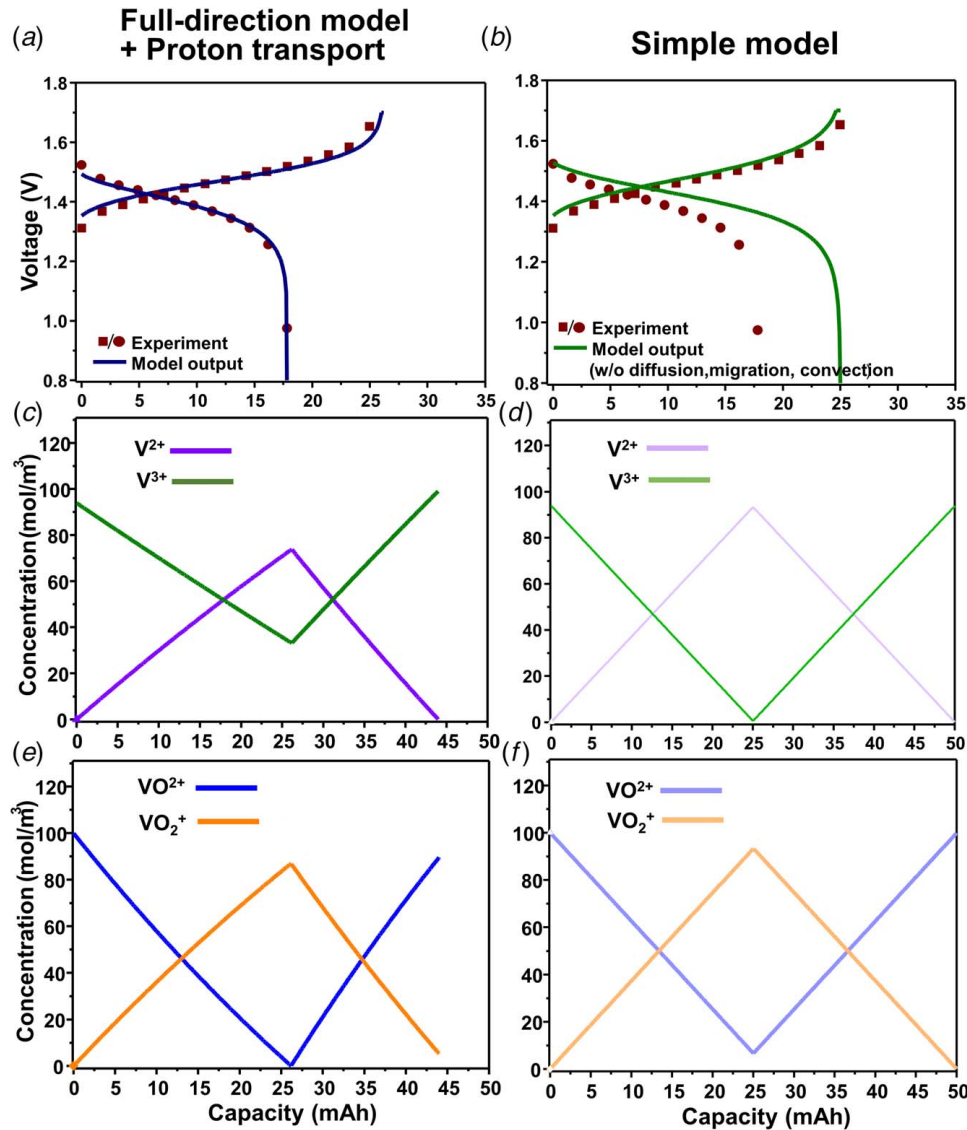
presents the comparison of voltage profiles between the model output and the experimental data, and Figs. 9(b) and 9(c) show the predicted concentration of V^{2+}, V^{3+}, VO^{2+}, and VO_2^+ ions of the batch cell system having Nafion® XL membrane. Like the Nafion® 115 system, the changes in concentration of V^{2+}/V^{3+} ions are smaller than that of VO^{2+}/VO_2^+ ions during charging. The imbalance of vanadium ion concentration between the positive and negative electrolytes causes capacity loss of VRBC systems. The imbalance of the Nafion® XL system is more severe than that of Nafion® 115. In Fig. 9(b), one of the observed phenomena is that the change in concentration of V^{2+} ions follows a typical behavior of vanadium redox flow batteries, but the concentration of V^{3+} ions barely changes during charge. Initially, the concentration of V^{3+} ions slightly increases and then begins to decrease. This is because the applied C-rate is significantly lower than that of typical vanadium redox flow battery systems. The low applied C-rate reduces the consumption rate of V^{3+} ions at the electrode. Also, the estimated diffusion coefficient of V^{3+} ions is smaller than that of VO^{2+} and VO_2^+ ions. As a result, the entering rate of V^{3+} ions through the membrane by the side reaction of VO^{2+} and VO_2^+ ions is higher than the sum of the rate of consumption of V^{3+} ions at the negative electrode and flowing-out rate of V^{3+} ions to the opposite electrolyte. This is the reason that the concentration of V^{3+} ions increases initially. Meanwhile, in the positive electrolyte, the concentration of VO_2^+ ion increases, and the concentration of VO^{2+} ions decreases during the charging process. This affects the entering rate of V^{3+} ions through the membrane from the positive electrolyte. According to the result of the parameter estimation, the diffusion coefficient of VO^{2+} ions through the membrane is higher than that of other ions, and the changes in the concentration of VO^{2+} and VO_2^+ ions in the positive electrolyte lead to a reduction in the amount of V^{3+} ions entering. This causes a decrease in the concentration of V^{3+} ions in the negative electrolyte. Therefore, the concentration of V^{3+} ions begins to decrease after a certain time.

- *Sensitivity analysis for the initial guess*: For the Nafion® XL system, the optimal values of diffusion coefficients from different initial guesses are more sensitive compared with optimal values for the Nafion® 115 system (see Table 9). Diffusion coefficients of VO^{2+} and VO_2^+ ions are relatively stable compared with diffusion coefficients of V^{2+} and V^{3+} ions.

In most cases of VO^{2+} and VO_2^+ ions, the optimal values were estimated as $\pm 15\%$ deviation from the initial guess variations of the other parameters. However, the diffusion

Table 8 Estimated parameters of all-vanadium redox batch cell systems (full-direction model)

Symbol	Parameter	Lower bound	Upper bound	Initial guess	95% Confidence interval	Final value	Units
$R_{cell\text{-}mem}$	Resistance excluding the membrane resistance	0	5	2	2.93–3.03	2.98	Ω
k_c	Rate constant at positive electrode	0.20×10^{-6}	4.04×10^{-6}	1.02×10^{-6}	1.07–1.19×10^{-6}	1.13×10^{-6}	$m^2\ s^{-1}$
k_a	Rate constant at negative electrode	3.56×10^{-7}	5.29×10^{-6}	1.37×10^{-6}	1.06–1.21×10^{-6}	1.13×10^{-6}	$m^2\ s^{-1}$
E'_0	Formal potential	1.26	1.49	1.35	1.34–1.35	1.35	V
D_{H^+}	H^+ diffusion coefficient of Nafion® 115	1.03×10^{-11}	1.02×10^{-9}	1.03×10^{-10}	9.93×10^{-11} to 1×10^{-10}	1×10^{-10}	$m^2\ s^{-1}$
	Nafion® XL	3.09×10^{-11}	2.52×10^{-9}	2.79×10^{-10}	4.32×10^{-11} to 8.84×10^{-10}	1.66×10^{-10}	$m^2\ s^{-1}$
$D_{V^{2+}}$	V^{2+} diffusion coefficient for Nafion® XL	1.26×10^{-13}	2.8×10^{-11}	1.88×10^{-12}	3.02×10^{-14} to 2.58×10^{-11}	0.88×10^{-12}	$m^2\ s^{-1}$
$D_{V^{3+}}$	V^{3+} diffusion coefficient for Nafion® XL	1.26×10^{-13}	2.8×10^{-11}	1.88×10^{-12}	9.37×10^{-13} to 1.73×10^{-12}	1.27×10^{-12}	$m^2\ s^{-1}$
$D_{VO^{2+}}$	VO^{2+} diffusion coefficient for Nafion® XL	8.2×10^{-13}	1.29×10^{-10}	1.03×10^{-11}	8.58×10^{-12} to 1.21×10^{-11}	1.02×10^{-11}	$m^2\ s^{-1}$
$D_{VO_2^+}$	VO_2^+ diffusion coefficient for Nafion® XL	3.79×10^{-13}	6.88×10^{-11}	5.11×10^{-12}	4.09×10^{-12} to 5.33×10^{-12}	4.67×10^{-12}	$m^2\ s^{-1}$

Fig. 8 Comparison of voltage and predicted concentration profiles between the full-direction model including the proton transport and the simple model for the batch cell system equipped with the Nafion® 115 membrane at C/30. (Experimental data: charge (wine color and filled square dots), discharge (wine color and filled circle), the full-direction model: blue straight line, and the simple model: green straight line.) (a) Full-direction model including the proton transport versus experimental data, (b) simple model versus experimental data, (c) V^{2+} (purple) and V^{3+} (green) concentration profiles from the VRBC model at C/30, (d) V^{2+} (light purple) and V^{3+} (light green) concentration profiles from the simple model at C/30, (e) VO^{2+} (blue) and VO_2^+ (orange) concentration profiles from the VRBC model at C/30, and (f) VO^{2+} (light blue) and VO_2^+ (light orange color) concentration profiles from the simple model at C/30. An imbalance of the vanadium ion concentration between the positive and negative electrolytes causes capacity loss of VRBC/VRFB systems and the simple model: green straight line).

Table 9 Sensitivity analysis for initial guesses

Parameter	Original initial guess	Original optimal value	Optimal value from the initial guess variation				
Nafion® 115 system			Initial guess variation				
			$k_a \pm 10\%$	$k_c \pm 10\%$	$E_0' \pm 10\%$	$R_{cell\text{-}mem} \pm 10\%$	$D_{H^+} \pm 10\%$
Rate constant at negative electrode $(k_a) \times 10^{-6}$	1.37	1.13	1.06–1.61	1.05–1.17	0.91–1.33	1.14–1.18	1.18–1.33
Rate constant at positive electrode $(k_c) \times 10^{-6}$	1.02	1.13	0.91–1.28	1.03–1.26	0.96–1.32	1.05–1.14	1.04–1.10
Formal potential (E_0')	1.35	1.35	1.35–1.35	1.35–1.35	1.35–1.35	1.35–1.35	1.35–1.35
Resistance excluding the membrane resistance $(R_{cell\text{-}mem})$	2	2.98	1.36–4.97	0.40–5.00	1.17–2.06	1.72–3.24	1.64–5.00
H⁺ diffusion coefficient $(D_{H^+}) \times 10^{-10}$	1.03	1	1–1	1–1	1–1	1–1	1–1
Nafion® XL system			Initial guess variation				
			$D_{V^{2+}} \pm 10\%$	$D_{V^{3+}} \pm 10\%$	$D_{VO^{2+}} \pm 10\%$	$D_{VO_2^+} \pm 10\%$	$D_{H^+} \pm 10\%$
V²⁺ diffusion coefficient for Nafion® XL $(D_{V^{2+}}) \times 10^{-12}$	1.88	0.88	0.22–1.21	0.13–1.69	0.13–0.25	0.13–1.41	0.13–1.52
V³⁺ diffusion coefficient for Nafion® XL $(D_{V^{3+}}) \times 10^{-12}$	1.88	1.27	1.10–1.42	1.06–1.86	1.13–1.45	1.15–1.73	0.95–1.67
VO²⁺ diffusion coefficient for Nafion® XL $(D_{VO^{2+}}) \times 10^{-11}$	1.03	1.02	0.48–0.97	0.97–1.04	0.98–1.07	1.00–1.04	0.95–1.01
VO₂⁺ diffusion coefficient for Nafion® XL $(D_{VO_2^+}) \times 10^{-12}$	5.11	4.67	4.77–4.94	4.68–5.08	4.60–5.00	4.5–5.23	4.76–5.15
H⁺ diffusion coefficient $(D_{H^+}) \times 10^{-10}$	2.79	1.66	1.68~1.93	1.74~2.42	1.96~2.84	1.65~2.86	1.67~2.31

coefficients of V²⁺ and V³⁺ ions were estimated to be considerable difference depending on the initial guess variation. In the case of the Nafion® XL system, therefore, it is more important to estimate parameters by the proper initial guess.

Uniqueness Issue With a Systems Approach

In most optimization methods for battery system simulations, it is required to identify appropriate initial guesses that provide model outputs, which are close to the experimental data [33]. However, parameter estimation techniques pose the following fundamental question: How would one know if a set of estimated values is unique? In other words, how would one convince if the converged values are the global minimum? If not, would there be multiple sets of parameter values that would provide similar MSEs? The answers and efforts to mitigate theses doubts help build a better battery system coupling with parameter estimation techniques. For example, the order of magnitude of the diffusivity of vanadium ionic species for the Nafion® XL membrane was estimated as $VO^{2+} > VO_2^+ > V^{3+} > V^{2+}$ in the previous section. However, the information on diffusivities of the vanadium ionic species for the Nafion® XL membrane is not available from the literature, and how would the converged parameters be confirmed to be correct values using a systems approach?

Currently, most global optimization techniques for battery simulations cannot guarantee the global minimum [33]. In parameter estimation, when a black-box model is used to simulate parameters and called with an optimizer, a global optimum cannot be guaranteed [33]. Therefore, one of the current approaches of dealing with this issue is to adopt more experimental data including different C-rates and confirm them with model outputs [34,35]. Another way to mitigate the uncertainties of the converged values is to calculate the confidence interval.

Different C-rates. The estimated parameters in the previous step were applied to the system at higher C-rates (C/20), and a good agreement has been observed for both Nafion® 115 and Nafion® XL systems, having the low value of MSEs, as shown in Fig. 10. The MSE of the Nafion® 115 and Nafion® XL system at C/20 is obtained as 2.67 mV and 16.49 mV, respectively. More experimental data will be utilized for parameter estimation studies of redox flow batteries to further improve the system reliability in our future work.

Confidence Interval. The confidence interval is defined by an upper and lower limit, and within the confidence interval, the converged value is considered to be a statistically true value with a predefined level of confidence [13]. The small confidence interval model contains a smaller design uncertainty for the converged parameters [13]. The 95% confidence interval can be calculated as follows [26]:

$$\mathbf{p}_{opt} - t_{95\%} S_E \sqrt{a_{ii}} \leq \mathbf{p} \leq \mathbf{p}_{opt} + t_{95\%} S_E \sqrt{a_{ii}} \qquad (3.M)$$

where $\boldsymbol{p}_{opt}$ is the vector of converged parameters, $t_{95\%}$ (=1.69) is the value of Student's t-distribution with $(N - n_p)$ degrees of freedom, and the value of standard deviation ($= S_E$) is a square root of MSE (see Eq. (2.M)).

The vector of a_{ii} is the ith diagonal element of the inverse matrix of the transpose Jacobian multiplied by the Jacobian for parameter estimation, which is described as Eq. (4.M).

$$(J^T \cdot J)^{-1}, \quad J = \left(\frac{\Delta V}{\Delta p_i}\right)_j = \left(\frac{V(p_{opt,i} + \Delta p_i) - V(p_{opt,i})}{\Delta p_i}\right)_j \quad (4.M)$$

The i is the order of the estimating parameters, the j is the order of the experimental data point, J is the Jacobian, J^T is the transpose Jacobian, and Δp_i (=10^{-12}) is a change in the value of parameters. For this convergence interval calculation, the numerical Jacobian is calculated, which can be obtained using results from the computational software solver. The 95% confidence intervals for each parameter are summarized in Table 8, and values in Table 8 were rounded off to the third decimal place.

- *Nafion® 115 system*: The 95% confidence intervals for the rate constants at the positive and negative electrodes, the cell resistance excluding the membrane resistance, the diffusion coefficient of protons, and the formal potential are 1.07×10^{-6} to 1.19×10^{-6} m/s, 1.06×10^{-6} to 1.21×10^{-6} m/s, 2.93–3.03 Ω, 9.93×10^{-11} to 1×10^{-10} m²/s, and 1.34–1.35 V, respectively.
- *Nafion® XL system*: The 95% confidence interval for diffusion coefficients of V²⁺, V³⁺, VO²⁺, VO₂⁺, and protons are 3.02×10^{-14} to 2.58×10^{-11} m²/s, 9.37×10^{-13} to 1.73×10^{-12} m²/s, 8.58×10^{-12} to 1.21×10^{-11} m²/s, 4.09×10^{-12} to 5.33×10^{-12} m²/s, and 4.32×10^{-11} to 8.84×10^{-10} m²/s, respectively.

Open Source Platform

Another possible way to confirm the uniqueness of the estimated parameters is to compare the converged values from different
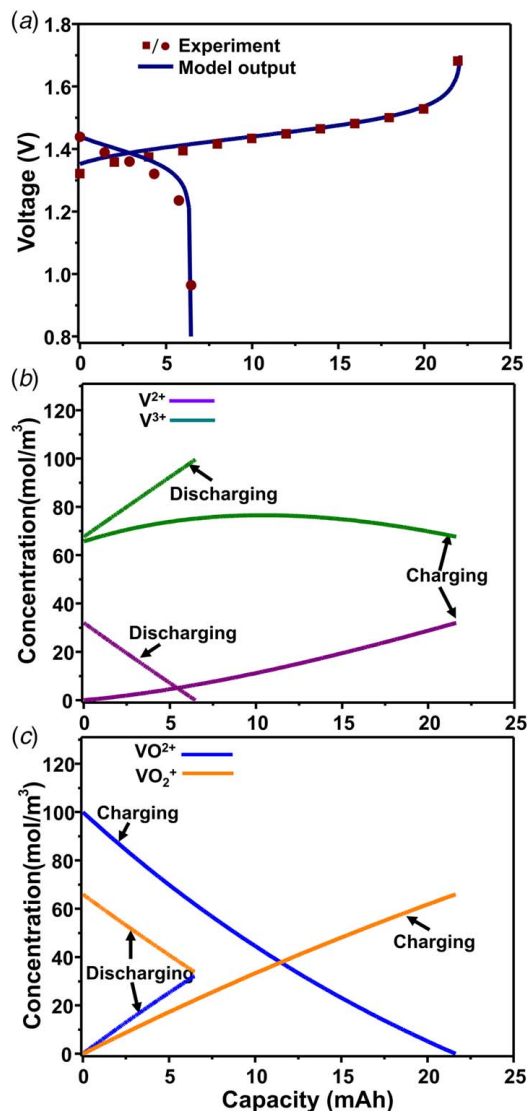
Fig. 9 Comparison of voltage profiles between model outputs and experimental data, and predicted vanadium ion concentrations versus capacity, for the batch cell system including the Nafion® XL membrane at the first cycle. The batch cell system is charged first and then discharged. (a) Voltage profiles from experiment data (charge: wine color and filled square, discharge: wine color and filled circle) and model outputs (blue straight line) at C/30, (b) V^{2+} (purple) and V^{3+} (green) concentration profiles at C/30, and (c) VO^{2+} (blue) and VO_2^+ (orange) concentration profiles at C/30. Parameters were estimated at C/30 based on cell system parameters predetermined in the Nafion® 115 system, minimizing the mean of sum-of-squared differences between the model and experiment outputs.

models describing the same system. The benefits and usability of this proposed approach can be accelerated and maximized through an open source platform provided in this paper (see Fig. 3). The open source platform for models, experimental database, and estimation techniques enable users to continuously modify models with detailed physics, additional experimental data, and more optimizers. By doing this, users can arrive at robust optimization approaches. In an open source platform, executable files, source codes, and experimental data are also provided, so that the proposed approach can be pragmatically implemented from users' point of view (see the Appendix).

Target Users. The executable files were designed for experimental researchers who are not familiar with mathematical
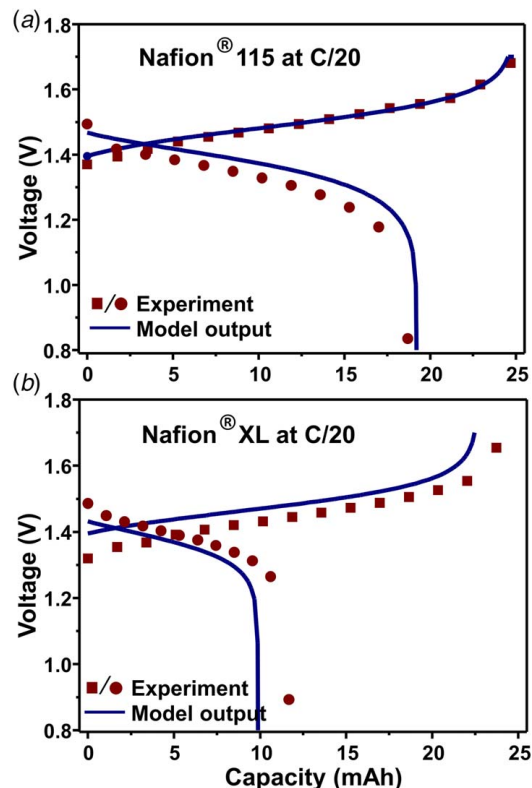
Fig. 10 Comparison of voltage profiles between model outputs and experimental data from the batch cell system at C/20. Voltage profiles of (a) the Nafion® 115 system and (b) the Nafion® XL system (Experimental data: wine color and filled square dots, VRBC model outputs: blue straight plot).

approaches or have the necessary computational infrastructure. Also, the source codes can be used by both modelers and experimental researchers to understand redox flow cell models and optimization approaches. Most of the literature on parameter estimation of redox flow batteries only provide model equations, estimation methods, and simulation and estimation results [36–38]. In those cases, however, if users want to estimate parameters of the redox battery system by following a way of estimation published in the literature, they need to install the specific computational software, write down model equations, and reproduce parameter estimation techniques. Although parameter estimation is a very active area of research in practical applications, this process is not an efficient way from a practical point of view. To resolve this issue, we provide executable files where the original programs are written in FORTRAN. The executable files can be used as an optimization tool to quickly address the parameter estimation problems for the redox battery systems. For example, the executable files allow users to estimate model parameters by simply providing experimental conditions (e.g., applied current, voltage data, and time intervals) and bounds for the parameters. Users can execute the file without any special computational requirement including any software installation and a priori programming knowledge. This enables users to easily understand VRBC/VRFB models and parameter estimation approaches. The detailed instruction of the executable files is explained in the Appendix.

Solver and Optimization. The executable files were generated after compiling the model equation files written in FORTRAN and integrated the same with the open source DAE solver package with zero crossing (DASKR) [39] and sequential least squares programming (SLSQP) [23]. The SLSQP algorithm includes the Han-Powell quasi-Newton method, and it can identify and optimize the battery performance with high speed and accuracy [27,40]. In this

paper, the optimization algorithm was run to adopt high accuracy ($\sim10^{-9}$) and a maximum of 1000 iterations.

Converged Parameters. The same initial guesses of the parameters presented in the previous section of this paper and adjusted bounds were used for the executable files. The difference of most converged parameters optimized by NLPsolve in Maple and open source platform of SLSQP with DASKR interface was found to be less than 10%. While using the SLSQP optimization, the converged parameters of the Nafion® 115 system for rate constants at the positive and negative electrodes, the cell resistance excluding the membrane resistance, the diffusion coefficient of protons, and the formal potential are found as 1.01×10^{-6} m/s, 1.37×10^{-6} m/s, $2\,\Omega$, 1.02×10^{-10} m/s, and 1.39 V, respectively. The converged parameters of the Nafion® XL system for the diffusion coefficients of V^{2+}, V^{3+}, VO^{2+}, VO_2^+, and protons are found as 1.92×10^{-12} m²/s, 1.94×10^{-12} m²/s, 1.24×10^{-11} m²/s, 4.78×10^{-12} m²/s, and 2.78×10^{-10} m²/s, respectively.

Conclusions and Perspectives

This work is an attempt to estimate all the parameters of VRBC systems using a zero-dimensional physics-based models formulated by a systems approach. This model includes mass balance equations of vanadium ions and protons in addition to the other equations covering the aspects of cell voltage, overpotential, and the membrane conductivity. This work also illustrates that VRBC/VRFB systems can be studied and analyzed in details based on a systems approach. Source codes and executable files are provided, which enables users to continuously improve models and quickly estimate parameters of the VRBC system. The proposed approach of parameter estimation is very generic and can be extended for the estimation of parameters for other RFB models incorporating different chemistry as well as complexity (0-D to 3-D). High-fidelity models for redox flow batteries are highly nonlinear and multidimensional in nature, and the use of these models will allow for more precise estimation of battery performance [41]. This study describes vanadium ions' behavior of the redox battery system, but other chemical species, such as sulfate and hydrogen sulfate, can also be included to achieve better prediction and accuracy of the model [6,12]. The proposed work includes ion transport through only the membrane using bulk solutions at the positive and negative electrolytes, but multidimensional models can include ion transport across entire cell (e.g., electrolytes, membranes, and electrodes). The proposed estimation approach will be implemented over full C-rates using more detailed models involving more ions and physics in the next study.

An efficient way of combining physics-based electrochemical models and parameters estimation techniques can facilitate the research on large-scale energy storage technologies, which are indispensable for the success and growth of intermittent sources of energy. For instance, the current practice in the grid/microgrid control systems is to utilize empirical battery models regardless of the type of the batteries [42]. Extended battery life and reduction in the size of RFBs, which are two of the most critical factors in the battery control system, can be achieved better if these empirical battery models are replaced with physics-based electrochemical models. The physics-based models have the power of predicting the battery performance and internal states accurately. With such detailed models, an efficient equation-based PV-Battery microgrid framework was recently developed to be able to simulate the entire microgrid components including physics-based battery models in real time, and the framework can implement any kind of physics-based electrochemical battery models [43]. Once the specific battery models are incorporated into the efficient equation-based microgrid framework, an important task is to estimate the parameters used in the model. The values of these parameters need updating at regular intervals to reflect the change in battery behavior over the cycles of charging/discharging. This enables the

models to have accurate predictions for several states of battery parameters, leading to a better prediction of battery usability, life, and improved safety. It also helps analyze and study the kinetics, transport phenomena, and capacity fade/degradation of the flow cell. However, several attempts to estimate the states and parameters of the VRFB system have been made using empirical/equivalent circuit-based models, which do not include detailed physics of the battery [36–38]. The proposed parameter estimation technique can be used to track the effects of capacity loss/fade. As we mentioned earlier, one of the main reasons of the redox batteries' capacity loss/fade is ions' crossover through the membrane [4], and this can be linked to transport and kinetic parameters.

Appendix

Note 1. Source Codes, Executable Files, and Text Files. There are two sets of source codes, executable files, and text files for the Nafion® 115 and the Nafion® XL systems. They are prepared to run on any Windows-based PC environment. Each set contains source codes, an executable file, and five text files. All relevant files can be downloaded directly from the Subramanian group's website as a zip file.[9] Once the zip files are downloaded, unzip all the files into the same folder. Below is the detailed instruction.

The Nafion® 115 System. The executable file ("Estimation_Nafion® 115 system.exe") in the zip file can estimate five parameters of the Nafion® 115 system: rate constants at anode and cathode, the cell resistance excluding the membrane resistance, the diffusion coefficient of protons, and the formal potential. The executable file uses one set of CC-CV charging and one set of CC discharging profiles and text files for specifying the experimental and model conditions.

(1) *Experimental conditions*: While specifying the experimental conditions, information such as (i) the value of applied current, (ii) the regular time interval for a profile, and (iii) the number of voltage data used for parameter estimation exercise are required. Users can enter their own experimental conditions to the text file called "Experimental conditions.txt." For the parameter estimation exercise carried out here, the following information has been entered. The first row is provided to enter values of applied currents for CC charging and CC discharging for Nafion® 115 system at one C-rate. The provide text file contains values such as 0.000893 (C/30) for the first row. The second and third

---

[9]http://depts.washington.edu/maple/VRBC.html

Table 10 Experimental data for flow battery and batch cell systems

	Operating condition	Electrolyte	Electrode	Separator	Flow rate	Flow Field
Experimental data for flow battery systems						
Experimental data set 1	CC charging/discharging (0.5 A)	1.7 M $VOSO_4$, 3.3 M H_2SO_4	Carbon felt	Nafion® 115	5 ml/min	10 cm^2, serpentine
Experimental data set 2	CC charging/discharging (0.25 A)	1.7 M $VOSO_4$, 3.3 M H_2SO_4	Carbon felt	Nafion® XL	5 ml/min	10 cm^2, serpentine
Experimental data for batch cell systems						
Experimental data set 3	CC-CV charging/discharging (C/10, C/20, C/30)	0.1 M $VOSO_4$, 4 M H_2SO_4	Graphite	Nafion® 115	N/A	H-cell
Experimental data set 4	CC charging/discharging (C/20, C/30)	0.1 M $VOSO_4$, 4 M H_2SO_4	Graphite	Nafion® XL	N/A	H-cell

rows represent time intervals of CC charging and CC discharging at C/30 rate. In the uploaded text file, these time intervals were set as 513.67 and 362.46 s for the C/30 operation. In the last row, users need to enter the number of the experimental data used for parameter estimation exercise. In this case, this number has been entered as 200.

(2) *Voltage data*: Provide experimental voltage data at your C-rate (e.g., C/30) in the file called "Voltage data.txt." Note that the same number of experimental data was prepared for charging and discharging profiles. The first row represents the number of the experimental data. The second and third columns present voltage data for charging and discharging at C/30, respectively. Users can input their experimental data sequentially.

(3) *Bounds*: Provide bounds for estimating parameters in the "Bounds.txt" file. The first row represents the total number of bounds. After that, the lower and upper bounds for each of the five estimating parameters are given in this file as an 5 rows by 2 columns array. The parameter bounds are given in the following sequence: rate constants at anode and cathode, the formal potential, the diffusion coefficient of protons, and the cell resistance excluding the membrane resistance.

(4) *Initial guess*: Provide initial guesses for estimating parameters in the "Guess.txt" file. Five estimating parameters are given in this file as a 5 rows by 1 column array. The initial guesses are given in the following sequence: rate constants at anode and cathode, the formal potential, the diffusion coefficient of protons, and the cell resistance excluding the membrane resistance. This sequence is same as the above sequence for providing the bounds for the parameters.

(5) *Model condition*: Provide mathematical conditions such as the number of ordinary differential equations (ODEs) and algebraic equations (AE) and tolerance in the text file called "daskrinput.txt." The number of ODE, the number of AE, a relative tolerance, and absolute tolerance are presented sequentially.

(6) *Double click and run the execution file "Estimation_ Nafion® 115 system.exe"*: Upon clicking, a command line window will be opened, and the program will calculate the optimal values of parameters. Once finishing the calculation, the command window will be closed. No action required.

(7) *The optimization results for all the variables can be found in the "Estimated parameters.csv"*: The results will be given by the following sequence: rate constants at anode and cathode, the formal potential, the diffusion coefficient of protons, and the cell resistance excluding the membrane.

The Nafion® XL System. The second program ("Other membrane system.exe") can estimate diffusion coefficients of four vanadium ions and protons for other membranes. The protocol to execute the executable file is similar to the previous step.

(1) *Identify your experimental conditions*: Users can enter their own experimental conditions in the "Experimental

conditions.txt" file. In the uploaded text file, the first row represents a value of applied currents for CC charging for the Nafion® XL system at C/30. The second and third rows represent time intervals of CC charging and CC discharging. Here, the time interval was entered as 446.76 and 105.15 s for charging and discharging at C/30. In the fourth row, users need to enter the number of the experimental data. In the original file, the number of 200 experimental voltage data was used. From the fifth to the seventh rows, the information obtained in the Nafion® 115 system was used, i.e., the fifth and sixth rows represent rate constants at anode and cathode, the seventh row represents the cell resistance and the formal potential.

(2) *Bounds for estimating parameters are entered in the "Bounds.txt" file*: The total number of bounds is given in the first row. After that, the bounds are given as a 5 rows by 2 columns array, i.e., the lower and upper bounds are given for the estimating parameters in the following sequence: diffusion coefficients of V^{2+}, V^{3+}, VO^{2+}, and VO_2^+, and protons.

(3) *Voltage data*: Provide experimental voltage data at one C-rate in the file called "Voltage data.txt." Note that the same number of experimental data was prepared for charging and discharging profiles. The total number of the experimental data is given in the first row. After that, the first and second columns present the voltage data for charging and discharging at C/30, respectively. Users can input their experimental data sequentially.

(4) *Initial guess and model conditions*: Provide initial guesses for estimating parameters into the "Guess.txt" file. Five estimating parameters are given in this file as a 5 rows by 1 column array. The initial guesses are given in the following sequence: diffusion coefficients of V^{2+}, V^{3+}, VO^{2+}, and VO_2^+, and protons. Also, mathematical conditions including the number of ODE and AE and tolerance are provided. The text file called "daskrinput.txt" includes the number of ODE, the number of AE, a relative tolerance, and absolute tolerance sequentially.

(5) *Double click and run the executable file "Other membrane systems.exe"*: Upon clicking, a command line window is opened, and the program will calculate the optimal values of the parameters. Once finishing the calculation, the command window will be closed. No action required.

(6) *The optimization results for all the parameters can be found in the "Estimated parameters.csv"*: The results will be given by the following sequence: diffusion coefficients of V^{2+}, V^{3+}, VO^{2+}, and VO_2^+, and protons.

Note 2. Experimental Data for Batch Cell and Flow Battery Systems. Experimental data for batch cell and flow battery systems under different operating conditions are hosted on the Sandia National Laboratory website.[10] Table 10 describes specific information for each experimental data set. Users can utilize the experimental data to their redox flow battery models.

---

[10]https://www.sandia.gov/ess-ssl/data-repository/

References

[1] Cho, K. T., Ridgway, P., Weber, A. Z., Haussener, S., Battaglia, V., and Srinivasan, V., 2012, "High Performance Hydrogen/Bromine Redox Flow Battery for Grid-Scale Energy Storage," J. Electrochem. Soc., **159**(11), pp. A1806–A1815.

[2] iOs Services, 2016, "Redox Flow Batteries Charge Forward," http://www.iosgeo.com/en/news/news-from-our-clients/redox-flow-batteries-charge-forward/. Accessed July 15, 2017.

[3] Shah, A., Tangirala, R., Singh, R., Wills, R., and Walsh, F., 2011, "A Dynamic Unit Cell Model for the All-Vanadium Flow Battery," J. Electrochem. Soc., **158**(6), pp. A671–A677.

[4] Tang, A., Bao, J., and Skyllas-Kazacos, M., 2011, "Dynamic Modelling of the Effects of ion Diffusion and Side Reactions on the Capacity Loss for Vanadium Redox Flow Battery," J. Power Sources, **196**(24), pp. 10737–10747.

[5] Tang, A., Bao, J., and Skyllas-Kazacos, M., 2012, "Thermal Modelling of Battery Configuration and Self-Discharge Reactions in Vanadium Redox Flow Battery," J. Power Sources, **216**(Oct.), pp. 489–501.

[6] Boettcher, P. A., Agar, E., Dennison, C., and Kumbur, E. C., 2016, "Modeling of Ion Crossover in Vanadium Redox Flow Batteries: A Computationally-Efficient Lumped Parameter Approach for Extended Cycling," J. Electrochem. Soc., **163**(1), pp. A5244–A5252.

[7] Pugach, M., Kondratenko, M., Briola, S., and Bischi, A., 2018, "Zero Dimensional Dynamic Model of Vanadium Redox Flow Battery Cell Incorporating All Modes of Vanadium Ions Crossover," Appl. Energy, **226** (Sept.), pp. 560–569.

[8] Gandomi, Y. A., Zawodzinski, T. A., and Mench, M. M., 2014, "Concentrated Solution Model of Transport in All Vanadium Redox Flow Battery Membrane Separator," ECS Trans., **61**(13), pp. 23–32.

[9] Lei, Y., Zhang, B., Bai, B., and Zhao, T. S., 2015, "A Transient Electrochemical Model Incorporating the Donnan Effect for All-Vanadium Redox Flow Batteries," J. Power Sources, **299**(Dec.), pp. 202–211.

[10] Shah, A., Al-Fetlawi, H., and Walsh, F., 2010, "Dynamic Modelling of Hydrogen Evolution Effects in the All-Vanadium Redox Flow Battery," Electrochim. Acta, **55**(3), pp. 1125–1139.

[11] Al-Fetlawi, H., Shah, A., and Walsh, F., 2010, "Modelling the Effects of Oxygen Evolution in the All-Vanadium Redox Flow Battery," Electrochim. Acta, **55**(9), pp. 3192–3205.

[12] Knehr, K., Agar, E., Dennison, C., Kalidindi, A., and Kumbur, E., 2012, "A Transient Vanadium Flow Battery Model Incorporating Vanadium Crossover and Water Transport Through the Membrane," J. Electrochem. Soc., **159**(9), pp. A1446–A1459.

[13] Darling, R. M., Weber, A. Z., Tucker, M. C., and Perry, M. L., 2016, "The Influence of Electric Field on Crossover in Redox-Flow Batteries," J. Electrochem. Soc., **163**(1), pp. A5014–A5022.

[14] Pratt, H. D., Hudak, N. S., Fang, X., and Anderson, T. M., 2013, "A Polyoxometalate Flow Battery," J. Power Sources, **236**(Aug.), pp. 259–264.

[15] Wiedemann, E., Heintz, A., and Lichtenthaler, R., 1998, "Transport Properties of Vanadium Ions in Cation Exchange Membranes: Determination of Diffusion Coefficients Using a Dialysis Cell," J. Membr. Sci., **141**(2), pp. 215–221.

[16] Sun, C., Chen, J., Zhang, H., Han, X., and Luo, Q., 2010, "Investigations on Transfer of Water and Vanadium Ions Across Nafion Membrane in an Operating Vanadium Redox Flow Battery," J. Power Sources, **195**(3), pp. 890–897.

[17] Li, J., Wang, L., Lyu, C., Wang, H., and Liu, X., 2016, "New Method for Parameter Estimation of an Electrochemical-Thermal Coupling Model for LiCoO 2 Battery," J. Power Sources, **307**(Aug.), pp. 220–230.

[18] Skyllas-Kazacos, M., and Goh, L., 2012, "Modeling of Vanadium ion Diffusion Across the Ion Exchange Membrane in the Vanadium Redox Battery," J. Membr. Sci., **399**, pp. 43–48.

[19] Aaron, D., Sun, C.-N., Bright, M., Papandrew, A. B., Mench, M. M., and Zawodzinski, T. A., 2013, "In Situ Kinetics Studies in All-Vanadium Redox Flow Batteries," ECS Electrochem. Lett., **2**(3), pp. A29–A31.

[20] Miller, M., Bourke, A., Quill, N., Wainright, J., Lynch, R., Buckley, D., and Savinell, R., 2016, "Kinetic Study of Electrochemical Treatment of Carbon Fiber Microelectrodes Leading to In Situ Enhancement of Vanadium Flow Battery Efficiency," J. Electrochem. Soc., **163**(9), pp. A2095–A2102.

[21] Shi, S., Weber, A. Z., and Kusoglu, A., 2016, "Structure/Property Relationship of Nafion XL Composite Membranes," J. Membr. Sci., **516**(Oct.), pp. 123–134.

[22] Motupally, S., Becker, A. J., and Weidner, J. W., 2000, "Diffusion of Water in Nafion 115 Membranes," J. Electrochem. Soc., **147**(9), pp. 3171–3177.

[23] Kraft, D., 1988, "A Software Package for Sequential Quadratic Programming," Forschungsbericht-Deutsche Forschungs-und Versuchsanstalt fur Luft- und Raumfahrt.

[24] Weber, A. Z., Mench, M. M., Meyers, J. P., Ross, P. N., Gostick, J. T., and Liu, Q., 2011, "Redox Flow Batteries: A Review," J. Appl. Electrochem., **41**(10), pp. 1137–1164.

[25] Ramadesigan, V., Chen, K., Burns, N. A., Boovaragavan, V., Braatz, R. D., and Subramanian, V. R., 2011, "Parameter Estimation and Capacity Fade Analysis of Lithium-Ion Batteries Using Reformulated Models," J. Electrochem. Soc., **158**(9), pp. A1048–A1054.

[26] Santhanagopalan, S., Guo, Q., and White, R. E., 2007, "Parameter Estimation and Model Discrimination for a Lithium-Ion Cell," J. Electrochem. Soc., **154**(3), pp. A198–A206.

[27] Brelje, B. J., and Martins, J. R., 2018, "Development of a Conceptual Design Model for Aircraft Electric Propulsion With Efficient Gradients," AIAA/IEEE Electric Aircraft Technologies Symposium, Cincinnati, OH, July 9–11, p. 4979.

[28] Pintér, J. D., Linder, D., and Chin, P., 2006, "Global Optimization Toolbox for Maple: An Introduction With Illustrative Applications," Optim. Method. Softw., **21**(4), pp. 565–582.

[29] Levenspiel, O., 1999, "Chemical Reaction Engineering," Ind. Eng. Chem. Res., **38**(11), pp. 4140–4143.

[30] Yang, X.-G., Ye, Q., Cheng, P., and Zhao, T. S., 2015, "Effects of the Electric Field on Ion Crossover in Vanadium Redox Flow Batteries," Appl. Energy, **145**(May), pp. 306–319.

[31] Lei, Y., Zhang, B., Zhang, Z. H., Bai, B. F., and Zhao, T., 2018, "An Improved Model of Ion Selective Adsorption in Membrane and Its Application in Vanadium Redox Flow Batteries," Appl. Energy, **215**(Apr.), pp. 591–601.

[32] Verma, P., Maire, P., and Novák, P., 2010, "A Review of the Features and Analyses of the Solid Electrolyte Interphase in Li-Ion Batteries," Electrochim. Acta, **55**(22), pp. 6332–6341.

[33] Lee, S. B., Pratt, H. D., Anderson, T. M., Mitra, K., Chalamala, B. R., and Subramanian, V. R., 2018, "Estimation of Transport and Kinetic Parameters of Vanadium Redox Batteries Using Static Cells," ECS Trans., **85**(5), pp. 43–64.

[34] Li, J., Zou, L., Tian, F., Dong, X., Zou, Z., and Yang, H., 2016, "Parameter Identification of Lithium-Ion Batteries Model to Predict Discharge Behaviors Using Heuristic Algorithm," J. Electrochem. Soc., **163**(8), pp. A1646–A1652.

[35] Jokar, A., Rajabloo, B., Désilets, M., and Lacroix, M., 2016, "An Inverse Method for Estimating the Electrochemical Parameters of Lithium-Ion Batteries I. Methodology," J. Electrochem. Soc., **163**(14), pp. A2876–A2886.

[36] Wei, Z., Tseng, K. J., Wai, N., Lim, T. M., and Skyllas-Kazacos, M., 2016, "Adaptive Estimation of State of Charge and Capacity With Online Identified Battery Model for Vanadium Redox Flow Battery," J. Power Sources, **332** (Nov.), pp. 389–398.

[37] Wei, Z., Lim, T. M., Skyllas-Kazacos, M., Wai, N., and Tseng, K. J., 2016, "Online State of Charge and Model Parameter Co-Estimation Based on a Novel Multi-Timescale Estimator for Vanadium Redox Flow Battery," Appl. Energy, **172**(June), pp. 169–179.

[38] Fares, R. L., Meyers, J. P., and Webber, M. E., 2014, "A Dynamic Model-Based Estimate of the Value of a Vanadium Redox Flow Battery for Frequency Regulation in Texas," Appl. Energy, **113**(Jan.), pp. 189–198.

[39] Petzold, L. R., 1989, "Recent Developments in the Numerical Solution of Differential/Algebraic Systems," Comput. Method. Appl. Mech. Eng., **75**(1–3), pp. 77–89.

[40] Wendorff, A., Botero, E., and Alonso, J. J., 2016, "Comparing Different Off-the-Shelf Optimizers' Performance in Conceptual Aircraft Design," 17th AIAA/ISSMO Multidisciplinary Analysis and Optimization Conference, Washington DC, June 13–17, p. 3362.

[41] Lawder, M. T., Suthar, B., Northrop, P. W., De, S., Hoff, C. M., Leitermann, O., Crow, M. L., Santhanagopalan, S., and Subramanian, V. R., 2014, "Battery Energy Storage System (BESS) and Battery Management System (BMS) for Grid-Scale Applications," Proc. IEEE, **102**(6), pp. 1014–1030.

[42] Beck, D. A., Carothers, J. M., Subramanian, V. R., and Pfaendtner, J., 2016, "Data Science: Accelerating Innovation and Discovery in Chemical Engineering," AIChE J., **62**(5), pp. 1402–1416.

[43] Lee, S. B., Pathak, C., Ramadesigan, V., Gao, W., and Subramanian, V. R., 2017, "Direct, Efficient, and Real-Time Simulation of Physics-Based Battery Models for Stand-Alone PV-Battery Microgrids," J. Electrochem. Soc., **164**(11), pp. E3026–E3034.